DRIVERS OF CHANGE IN THE NORTH AMERICAN ELECTRIC GRID

BY

SAURAV MOHAPATRA

THESIS

Submitted in partial fulfillment of the requirements
for the degree of Master of Science in Electrical and Computer Engineering
in the Graduate College of the
University of Illinois at Urbana-Champaign, 2012

Urbana, Illinois

Adviser:

Professor Thomas J. Overbye

ABSTRACT

In the first part of this thesis, background material will be covered to motivate the research ideas being pursued in relation to electromechanical disturbance propagation, which is caused by an imbalance in power supply and demand at any location of an electric grid. The delay associated with this phenomenon is generally observed in large-scale interconnected power systems, and the impact of large changes in load or generation can be felt over a wide geographic area. A high penetration of solar and wind resources will tend to add more variability in generation, but also decrease the ratio between the total spinning inertia and power being produced. For the same amount of power imbalance, a larger frequency deviation will be observed in a system with higher renewable penetration. To understand the crux of this phenomenon, a relatively small 9-bus system is introduced. Transient analysis is carried out using non-linear and linear models to simulate a fault that causes a sudden disturbance to the power balance at one of the buses. Visualization of the transient response is provided, and a comparison of the time delays associated with the electromechanical disturbance propagation is presented for the 9-bus system. In the second part of this thesis, a literature review of utility-scale energy storage devices is presented, which have a symbiotic relationship with the integration of renewables to balance real power supply. Also, the aggregate effect of smart devices at the residential level is evaluated towards reactive power voltage support. These smart devices are becoming more common, and many of them already possess the hardware and software capabilities to implement reactive power injection control. In the near future, such devices would be dispersed over a large portion of the electric distribution network, thus making distributed reactive voltage support feasible. Network-level benefits of such a scheme are presented using a PowerWorld simulation. Applications are discussed, and a proposed control framework is simulated in Simulink for a single smart device.

To my family, for their love and support

and

in loving memory of . . .
my grandfather, Gokula Nanda Mahapatra (1927-2004),
my grandmother, Sita Mahapatra (1937-2010),
and my aunt, Dr. Gayatri Mahapatra (1957-2006)

ACKNOWLEDGMENTS

I am grateful for the support provided by the U.S. Department of Energy under award number DE-OE0000097, the Global Climate and Energy Project at Stanford University, and the National Science Foundation under award number 1128325.

I am thankful for the guidance from my adviser, and for his continued confidence in me.

My parents and sister have given me the strength to reach for the stars and chase my dreams – thank you very much!

To all my friends – your company, encouragement, and understanding have made this journey worthwhile. Despite many of you being on different continents, you are always on my mind.

TABLE OF CONTENTS

CHAPTER 1

THE NORTH AMERICAN ELECTRIC GRID

The North American electric grid is one of the largest and the most interconnected machines ever created. In terms of both the geographic area it covers and the amount of energy it carries, it is has been termed a marvel of 20^{th}

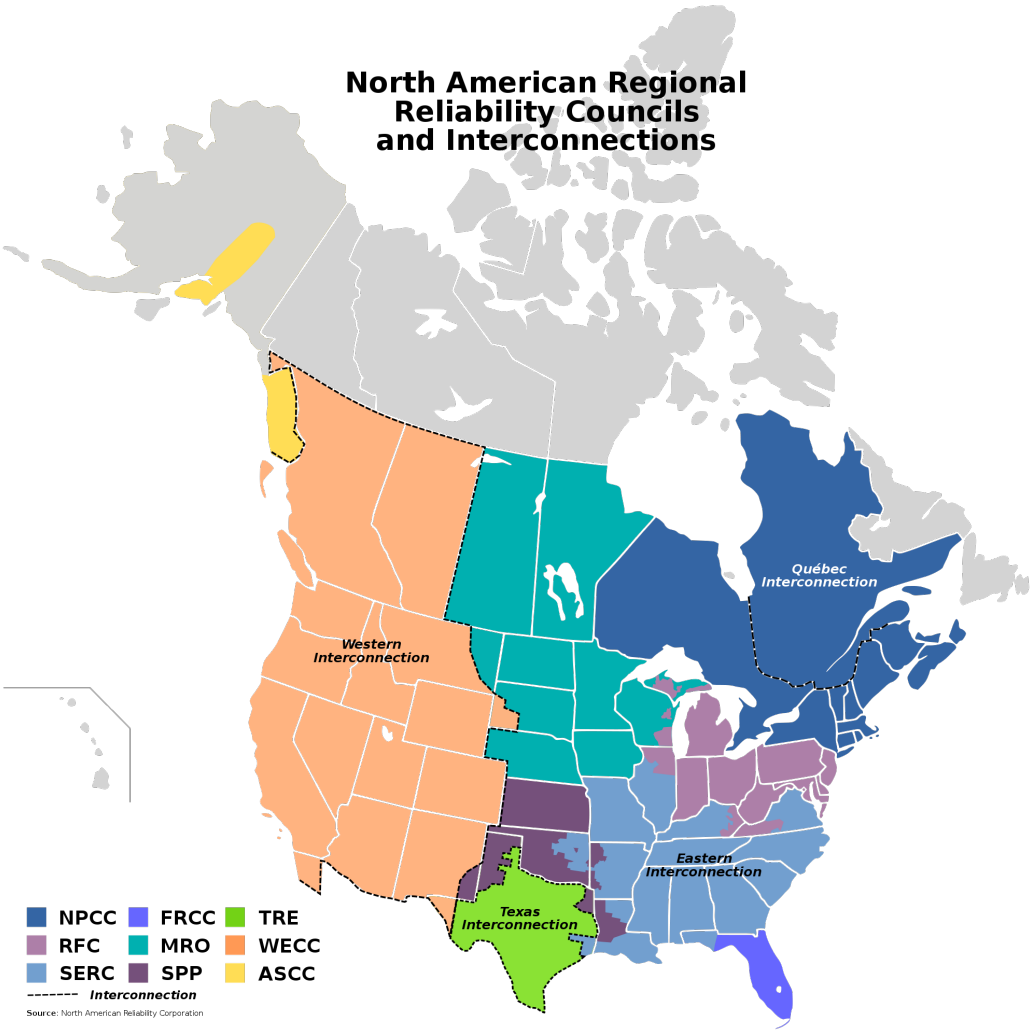

Figure 1.1: North American regional reliability councils and interconnections [1]

century engineering [2]. As seen in Figure 1.1, it consists of the Eastern Interconnection, Western Interconnection, Texas Interconnection and Quebec Interconnection. Each of these four large ac synchronous subsystems is operated at a nominal frequency of 60 Hz. There are back-to-back ac-dc-ac ties which allow for relatively small amounts of power to be transferred between these four interconnections. During steady-state operation, the frequency at two locations within the same interconnection is a very close match regardless of the geographic separation between them. However, if locations in different interconnections are compared, the frequency will not necessarily be as close. This is because the ac power system in each interconnection tries to maintain nominal frequency independent of other interconnections. Similarly, any disturbance (to the operating point) occurring within one of these interconnections is felt within the same interconnection, and has negligible impact on the others.

Before discussing the system level view of the North American electric grid, it is useful to understand the major components that make up power systems. Figure 1.2 is a rather simplistic representation of an electric power system; however, it gives a good pictorial view of the main building blocks. They are:

a) Generation

b) Transmission

c) Commercial and industrial business consumers

d) Distribution

e) Distribution automation services

f) Residential consumers

In a conventional ac power system, electricity is generated at power stations. It is then stepped-up to a higher voltage with the use of transformers. This higher transmission voltage allows electricity to be sent over longer distances and with lower energy losses in the transmission lines. Although Figure 1.2 shows a non-meshed network, the North American electric grid generally consists of meshed transmission networks. They stretch across several states and provinces. These vast transmission networks are like major

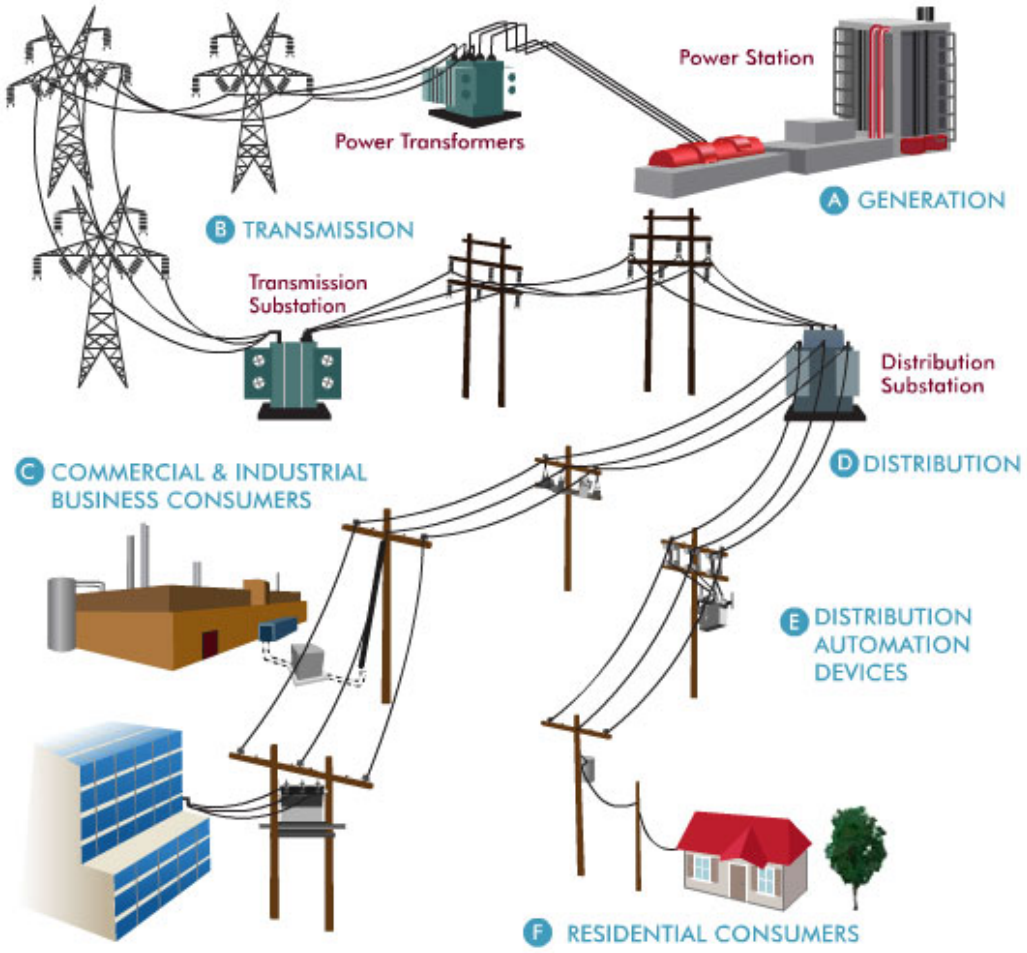

Figure 1.2: Pictorial representation of an electric power system [3]

highways which form the backbone of the grid, and support bulk transfer of electrical energy. Each city or town has one or more connections to the main transmission network through transmission and distribution substations which step-down the voltage. Beneath the layer of substations, lies the distribution network (usually at a lower voltage level than the transmission network). The distribution network is mainly radial and delivers electricity to both residential and commercial consumers. There are also several distribution automation devices within the distribution networks which monitor grid conditions, allow breaker switching actions, and provide reactive power support. Some of these distribution automation devices are remotely accessible to the grid operators.

In the U.S. the total generation capacity is slightly under 1 TW. In terms of electrical energy generation, most of it is derived from coal, natural gas, nu-

clear fuels and hydro plants. The remaining resources are petroleum, wood, wind, biomass, and solar, which make up a small fraction. The total electrical load in the U.S. varies throughout the day. There are daily, weekly, and seasonal patterns observed in load depending on which area of the electric grid is being studied. In general, different areas are known to achieve their peak demand of electricity at different times of the year.

Typical transmission voltages in the U.S. are 765, 500, 345, 230, 161, 138, and 69 kV. However, distribution lines are usually at lower voltages of 12.4 or 13.8 kV. In general, the aim is to transfer electrical energy from generation to load with as little energy loss as possible. This is where the high-voltage lines are useful in reducing losses over long distances. However due to safety concerns in populated areas, distribution lines are at lower voltages because they are easier to insulate and handle. Almost all high-power ac systems use a three-phase design which can transmit about twice as much power as an equivalent single-phase system.

As shown in Figure 1.1, there are regional reliability councils that work towards system resource adequacy and long-term planning reliability of the grid. However, from a operation standpoint, there are several balancing authorities which are in charge of portions of the interconnections to ensure real-time balance between power being generated and consumed in all parts of their respective areas. Several of these balancing authorities work together to ensure that power balance is maintained within an interconnection. The transmission lines which connect two balancing authority areas are known as tie-lines. These tie-lines help facilitate power transactions between two areas, which are contracts that can be for any amount of time duration at a particular price and power level. Balancing authorities also have several control measures for frequency control, which will be discussed in a later chapter.

The North American electric grid did not come into existence overnight, but is a machine which has been developed in stages. Advances in science, new challenges, a push towards better energy efficiency, and the integration of renewable energy sources are some of the key drivers of change today. The electric grid continues to evolve, and is under stress due to a gradual but imminent shift in its technical characteristics. Some of this is a result of policies (or a lack of them), but also due to development of next-generation technologies. In essence, there is a need for the electric grid to be "updated",

so that it can continue to support its consumers in a reliable and secure fashion.

This thesis will cover some of the key drivers of change from a technical perspective and touch upon areas of possible future research. Chapter 2 will delve deeper into the effects of large renewable energy resource additions which are expected to alter the grid's behavior during non-steady-state operation. After a discussion of background to set the context of the research, Chapter 3 will introduce a 9-bus system and present transient analysis aimed at understanding the time delay associated with electromechanical disturbance propagation. It is hoped that this research will provide insights into developing new tools to understand dynamic system behavior and help with real power balance. In Chapter 4, a literature review of utility-scale energy storage devices will be covered, which are crucial for the integration of renewable resources that are intermittent and can be unpredictable. Some of these energy storage technologies will help in mitigation strategies against the negative effects of a high degree of renewable penetration in the electric grid.

Chapter 5 discuss some of the new technologies (such as electric vehicles, and community energy storage devices) that are set to impact the grid in the near future. It will also cover a system-level view of the provision of reactive power support by smart devices, which can bring about systemwide benefits. As a continuation, Chapter 6 will present the simulation of a battery-inverter device which portrays a smart device that can be remotely instructed to provide reactive power voltage support. Lastly, Chapter 7 will consist of concluding remarks and future research.

CHAPTER 2

ELECTROMECHANICAL DISTURBANCE PROPAGATION

An electric power system broadly consists of generation, transmission, and distribution. The general flow of energy is from points of generation to points of consumption (i.e. loads), both of which are geographically dispersed throughout the power system. In the United States the nominal frequency of operation of the ac power system is 60 Hz. During steady-state operation, the amount of power being generated equals that being consumed plus losses in the system. This power balance is maintained at all locations of an energized electric power system. However, the steady-state operating point can be disturbed due to fluctuations in generation or load. As a result the frequency is affected, and this disturbance is felt throughout the power system. As seem in Figure 2.1, the balance can tip in either direction depending on the nature of the power imbalance, and directly affect the frequency. The propagation of this disturbance within the power system can be thought of as an electromechanical disturbance propagation.

As more renewable energy sources are added to the electric grid, there is expected to be higher levels of fluctuation in generation, and a decrease in the ratio between the total spinning inertia and power being produced. This will result in more dynamic behavior. Also, a greater frequency deviation is expected during large power imbalances. The propagation of these electromechanical disturbances has a finite time delay. Therefore it is of interest

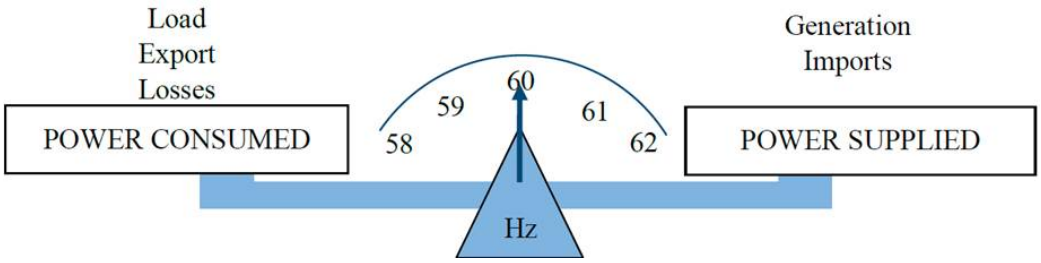

Figure 2.1: A diagram illustrating power balance [4]

to study this phenomenon for the following reasons:

i) To examine electromechanical disturbances in the electric grid, and better understand the time delay associated with this phenomenon.

ii) To aid in the integration of renewable energy sources.

iii) To create diagnostic tools for the electric grid, and interpret dynamic behavior of power systems.

Before diving into the analysis, background is presented to motivate the context of the research, and justify why the presence of more renewables can cause large-scale disturbances of greater magnitude. A simulation of the Western Interconnection is also discussed to show the occurrence of this phenomenon, and the associated time delay.

2.1 Background

Electromechanical disturbances can be caused due to a mismatch in generation and demand, which is the direct cause of frequency instability. However, frequency response (primary control), and regulation (secondary control) in the North American power systems enables sustaining the frequency within a narrow range around 60 Hz by continually reestablishing the power balance. Primary control (Table 2.1) occurs in the time frame of <1 minute, while secondary control occurs between 1-10 minutes of a disturbance in the power balance. It is essential to maintain frequency close to the nominal value because equipment in ac power systems is designed for a particular frequency. Over/under frequency can lead to their damage. The response of individual generators via governor control during frequency response does not restore

Table 2.1: Control continuum summary [4]

Control	Auxiliary service	Time frame	NERC standard
Primary	Frequency response	10-60 seconds	FRS-CSP1
Secondary	Regulation	1-10 minutes	CSP1-CPS2
Tertiary	Imbalances/reserves	10 minutes - hours	BAAL-DCS
Time	Time error correction	hours	TEC

nominal frequency. As a secondary measure, automatic generation control (AGC) kicks in to restore nominal frequency.

Studies have shown that there has been a significant shift from large, centralized power plants with large moments of inertia to small, more distributed and renewable power plants with much less moments of inertia [4], which are operating at their peak output levels. Although the moment of inertia is not the cause of frequency instability, the stored rotational kinetic energy acts as a buffer during power imbalances, which results in lower frequency deviations. The decrease in moment of inertia has resulted in a decline in the total rotational kinetic energy of the system, implying that larger and more geographically widespread frequency deviations can occur for the same amount of power imbalance. As more renewables come on-line, there will be a loss in governor response and spinning inertia. Apart from variability in generation from intermittent renewables, there is a concern about frequency stability of power systems due to lower system inertia.

Based on historic data, several low-frequency (i.e. $<$59.95 Hz) [5] and high-frequency (i.e. $>$60.05 Hz) [6] events have been observed in all four interconnections, and are on the rise. The report in [4] has attempted to correlate the increased number of larger and longer-lasting frequency deviations against the electricity market design and frequency control regulations. One of the technical causes for this in the Eastern Interconnection has been tracked and analyzed by the authors of [7] for a period of more than 15 years. They have calculated a value β, which is a constant of proportionality between the degree of power imbalance and the resulting frequency deviation. β is measured in MW/mHz, and the trend of β for the Eastern Interconnection is shown in Figure 2.2. This decline in β implies that a power imbalance of smaller magnitude is capable of causing a frequency deviation of 1 mHz. In other words, a larger frequency deviation can be expected for the same amount of power imbalance in the Eastern Interconnection. Since, there has been a push towards the integration of renewables all over North America, the same trend will occur in other interconnections.

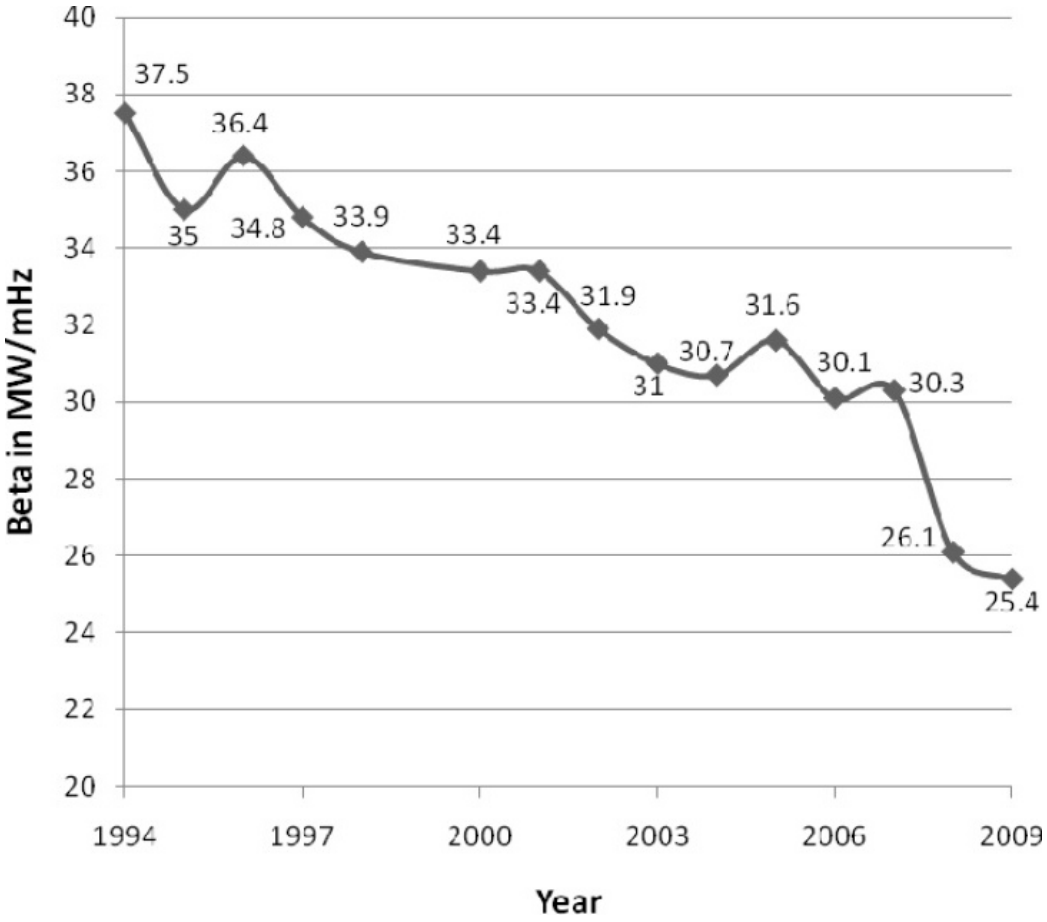

Figure 2.2: Mean β computed for each year from 1994 through 2009. Data is incomplete for the year 1999, so that year is omitted from this plot. [7]

2.2 Electromechanical disturbance propagation in the Western Interconnection

The Western Interconnection is the interconnected electrical power system that encompasses the provinces of Alberta and British Columbia (Canada), the northern portion of Baja California (Mexico), and portions of the 14 western states (U.S.) in between. Measurement data collected during large system events has shown delays in electromechanical disturbance propagation. A similar delay is also observed in a simulation of the WECC planning model.

It takes about 2.5 s for the frequency of buses in the North to fall below 59.95 Hz in response to a sudden loss of large generation in the southern part of the Western Interconnection (Figures 2.3 and 2.4). To make up for

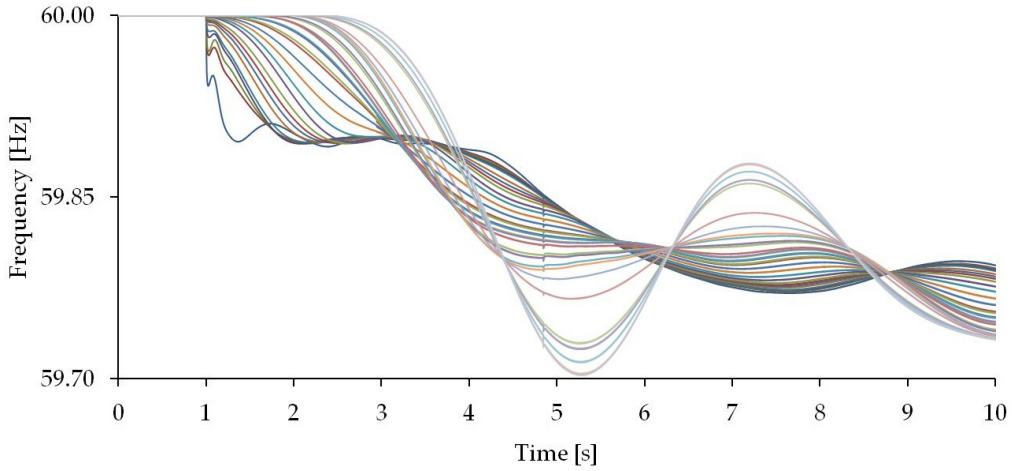

Figure 2.3: Frequency at selected buses in the WECC planning model in response to a large loss of generation in the southern part of the Western Interconnection

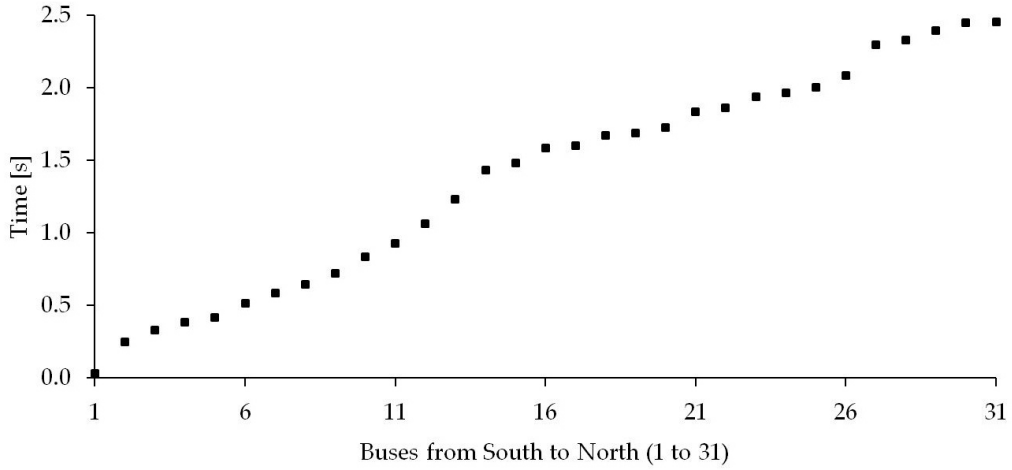

Figure 2.4: Time elapsed from the instance of the fault until frequency falls below 59.95 Hz at selected buses of the WECC planning model

the lack in generation, the power to supply the load is extracted from the rotational kinetic energy of the generators, and that reduces frequency. The delay is attributed to the rotational inertia of the generators (which resist the change), and the impedance of the transmission lines [8, 9, 10]. Studies have also shown that the speed of disturbance propagation in transmission networks is usually several hundred times lower than that in distribution networks [11].

2.3 Wide-area governor response

In the event of a sudden loss in generation at the southern part of the Western Interconnection, a plot of the bus frequencies corresponding to the post-fault transient response exhibits three key features. With reference to Figure 2.5, they are: (i) the time delay of the electromechanical disturbance propagation, (ii) the magnitude of the maximum frequency deviation, and (iii) the primary frequency response (i.e. governor response).

In an interconnected system, only a subset of all the generators participate in primary frequency response. For this subset, the governors of the respective generators regulate the mechanical power input based on a local frequency measurement. As seen in Figure 2.5, it takes about 2.5 s for the frequency of buses in the North to fall below 59.95 Hz in response to a sudden loss of large generation in the southern part of the Western Interconnection. The governors in the South are triggered earlier than those in the North, because the local frequency excursions occur at different points in time following the fault. Once the frequency disturbance is detected, the governors respond to restore power balance. In the case of the fault discussed above, the average value of frequencies, measured at different buses, reaches a minimum at about 10 s after the fault. Since the governors respond based on a local frequency measurement, their response can be somewhat myopic and sub-optimal from a system-level perspective. Overall, it takes >50 s for the

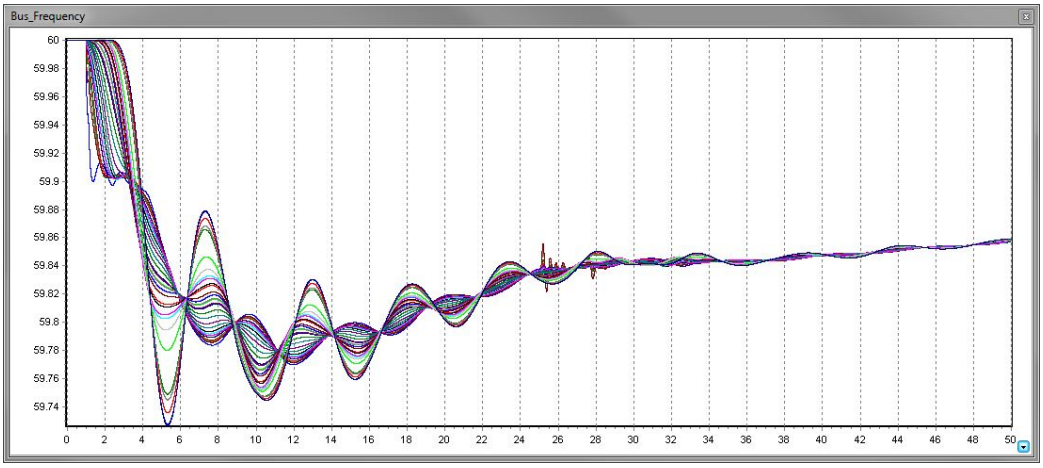

Figure 2.5: Frequency at selected buses in the WECC planning model in response to a large loss of generation in the southern part of the Western Interconnection (shows 0 to 50 s, with fault at 1 s)

frequency to creep up to a new steady-state value.

Apart from primary frequency response, there are also other forms of frequency control (Table 2.1) which play a role in restoring frequency to its nominal value. Secondary and tertiary controls are generally less myopic as their control signal is calculated based on areas under the purview of the respective balancing authorities. However, secondary, tertiary, and time controls have not been included in the simulation of the WECC planning model because they usually occur beyond the one minute time frame.

An idea for possible research could be the inclusion of a wide-area control signal, which would have the capability to trigger governor response in the same time frame as primary frequency response, even if the local frequency measurement has yet to deviate from the nominal value. If this idea were to be feasible, the time frame of primary frequency response would consist of two control actions: (i) Myopic governor response based on a local frequency measurement (MGR control), and (ii) Wide-area governor response based on a wide-area control signal (WGR control). It is possible that the wide-area control signal would be unique for each governor based on the degree of response of their respective MGR control, as well as their relative distance from buses whose frequency has already been disturbed by a fault. (This fault would be the trigger for primary frequency response in the overall system.)

In terms of the fault corresponding to Figure 2.5, MGR control for generators in the North is triggered after about 2.5 s of the fault. However, the idea discussed above would allow WGR control to be triggered prior to 2.5 s at generator buses in the North, and result in an earlier governor response. This would allow the system to take advantage of the disturbance propagation delay and trigger governor response over a wide-area, earlier than that shown in Figure 2.5.

A lower magnitude of frequency deviation and a faster restoration of a new steady-state could be some desirable outcomes of such a control scheme. However, there could be potential disadvantages such as premature over/under frequency response if the control scheme is not tuned correctly. Further work is necessary to develop the details of this hybrid MGR-WGR control scheme; however, the current state of computer processors, digital control technology and advanced telecommunication is promising for the realization of such a hybrid MGR-WGR control scheme.

2.4 The Western Interconnection in 2020

The regional entity responsible for coordinating and promoting the bulk electric system is the Western Electricity Coordinating Council (WECC). In the recently released 10-Year Regional Transmission Plan [12] by the WECC, predictions of load and generation have been discussed. In particular, renewable energy resource additions that are required to meet statutory *Renewable Portfolio Standards* (RPS) have been mentioned. RPS consist of regulations that requires an established level of production or purchase of energy from renewable energy sources.

Installed generation capacity in the Western Interconnection is expected to rise; however it is predicted that there will be a very small increase in dispatchable generation capacity. By 2020, most of the increase in capacity is expected to be from renewables. This totals to about 33,000 MW of additional renewable generation capacity which will be mainly nondispatchable, and will require balancing by conventional sources. Although the RPS goal varies between states, it is projected that renewables will form 17% of the annual total generation of the Western Interconnection in 2020 (Figure 2.6). Generation from wind and solar (Figure 2.7) will make up about 11% of the total annual generation. This will add variability in generation, and also re-

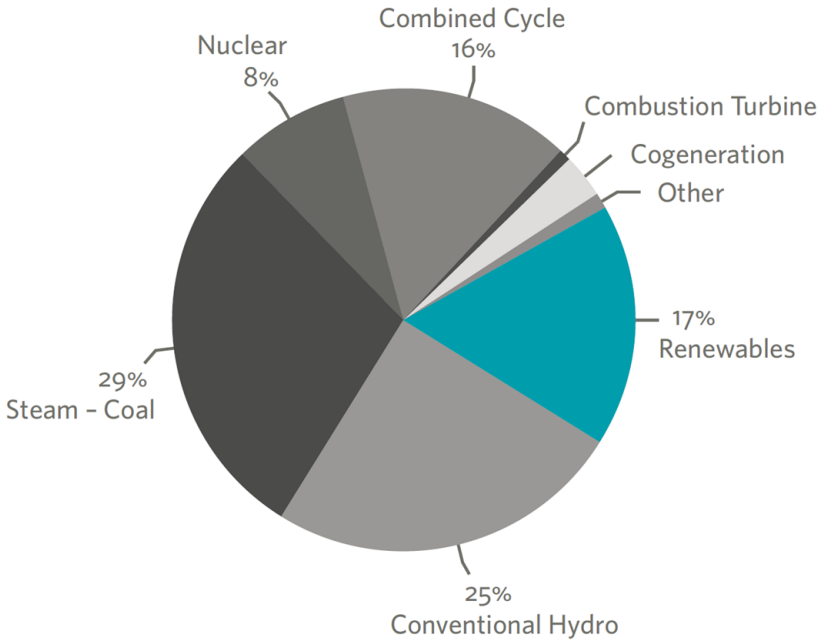

Figure 2.6: Percent of projected annual total generation by type in 2020 [12]

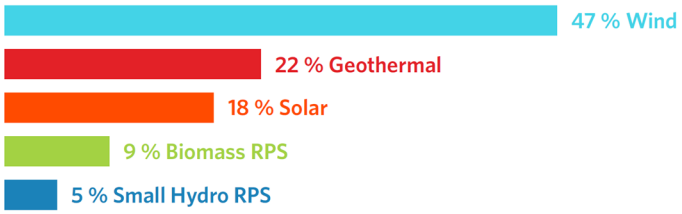

Figure 2.7: Projected annual renewable generation by type in 2020 (due to rounding, sum of percentages $\neq 100\%$) [12]

duce the ratio between rotational kinetic energy of spinning inertia and total generation. With better understanding of the time delay phenomenon, it may be possible to prevent geographically widespread frequency disturbances.

2.5 Forms of intermittent renewable energy

Wind turbines such as those shown in Figure 2.8 are becoming prevalent in several parts of the U.S. They are proving to be a good alternative to fossil fuels – available plentifully and without any emissions. The effects wind farms have on their local environment is far less compared to conventional power plants. Very often they are seen amidst agricultural land which is flat and open terrain. Wind farms can vary in size - from a few wind turbines to

Figure 2.8: Brazos wind farm [13]

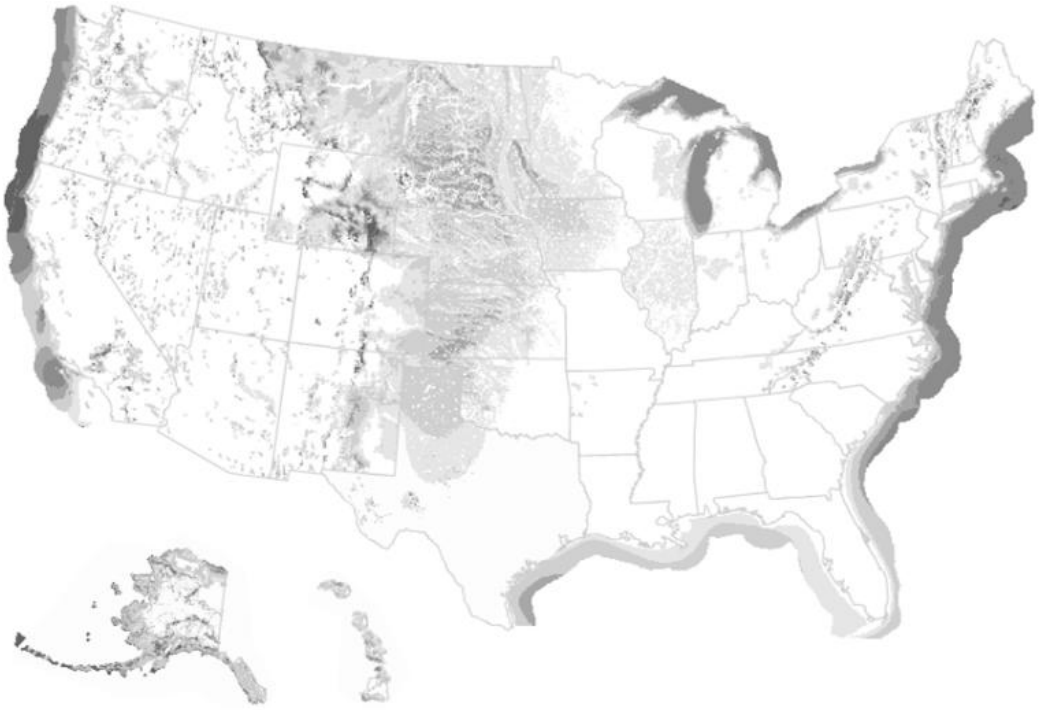

Figure 2.9: U.S. wind speeds map [14]

several hundred which can be connected to the nearest transmission network.

Figure 2.9 shows the average wind speeds in the U.S. The darker regions along the costs indicate higher wind speeds. These off-shore locations can yield greater energy due to the higher wind speeds. However, most of such places still remain unexplored because of the hefty costs associated with laying underground cables, building extremely durable wind turbines, wind speed intermmitency, maintenance, and safety concerns.

Solar-thermal plants, photo-voltaic plants, and solar water heating sites are the three main kinds of technologies that are in use today to harness the radiation of the sun and convert it to useful forms. Figure 2.10 shows one such installation in an arid region. Other technologies such as parabolic troughs, Fresnel troughs, solar towers, and parabolic dishes are considered as solar-thermal plants because they use the thermal steam cycle to drive a turbine which generates electricity.

Figure 2.11 shows a solar insolation map of the U.S. The darker regions receive higher solar radiation on average. However, just like wind, solar radiation can also fluctuate depending on time of day, weather, and time of year. Photovoltaic cells, which convert radiation directly to electrical

Figure 2.10: Nellis solar power plant [15]

energy, show an immediate drop in generation once there is a cloud-cover. Solar-thermal plants may be immune to such short-term cloud cover but will exhibit a similar drop in generation once there is insufficient heat to maintain high-pressure steam.

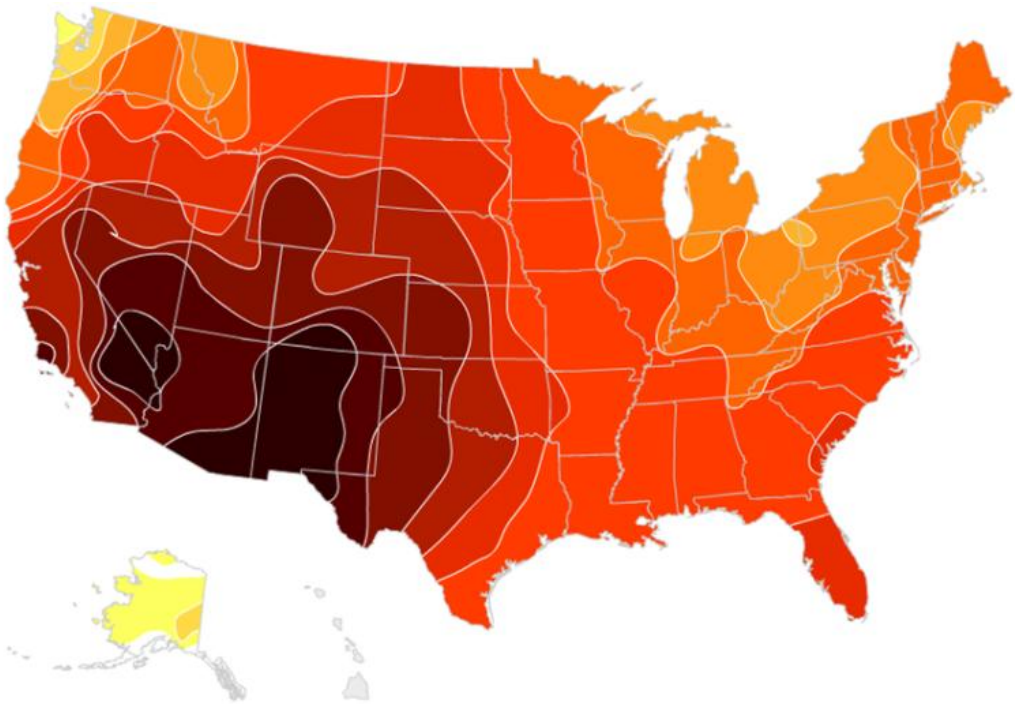

Figure 2.11: U.S. solar insolation map [14]

CHAPTER 3

A 9-BUS EXAMPLE

This chapter focuses on the transient analysis and visualization of electromechanical disturbance propagation in power systems. A 9-bus system is introduced to study electromechanical disturbance propagation. It is used to gain intuition into the crux of this phenomenon, and investigate the time delay associated with it. With reference to Figure 3.1, it has three areas – each with one generator and one online load (the load at bus 3 is offline, and is used as a fault for transient analysis). Classical machine models in equation (3.2) [16], and simple turbine-governor models in equation (3.3) (block diagram in Figure 3.2) [17] are used to represent system dynamics. Equation (3.1) defines the constant voltage, $E_i'^o$ and angle, $\delta_i'^o$ of the classical machine models. Lastly, equation (3.4) expresses the network algebraic constraints. Initial conditions are calculated from the solved power flow (Figure 3.1).

$$E_i'^o \triangleq \sqrt{(E_{di}'^o + (X_{qi}' - X_{di}')I_{qi}^o)^2) + (E_{qi}'^o)^2} \tag{3.1a}$$

$$\delta_i'^o \triangleq \tan^{-1}\left(\frac{E_{qi}'^o}{E_{di}'^o + (X_{qi}' - X_{di}')I_{qi}^o}\right) - \frac{\pi}{2} \tag{3.1b}$$

$$\frac{d\delta_i}{dt} = \omega_i - \omega_s \tag{3.2a}$$

$$\frac{2H_i}{\omega_s}\frac{d\omega_i}{dt} = T_{Mi} - \Re\left[E_i'^o e^{j(\delta_i - \delta_i'^o)}(I_{di} - jI_{qi})e^{-j(\delta_i - \frac{\pi}{2})}\right] \tag{3.2b}$$

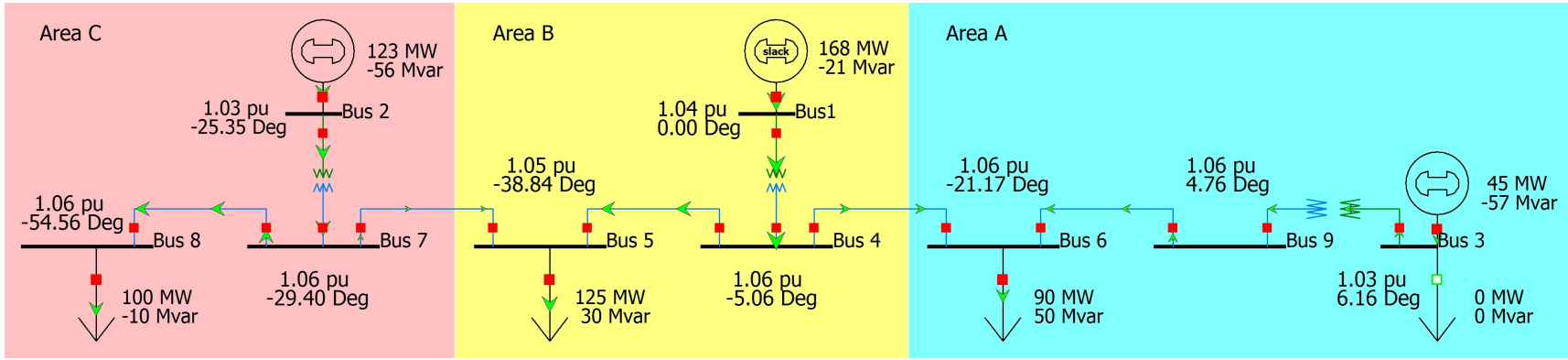

Figure 3.1: Oneline diagram of a 9-bus system with a solved power flow

$$T_{SVi}\frac{dP_{SVi}}{dt} = -P_{SVi} + P_{Ci} - \frac{1}{R_D}\left(\frac{w_i}{w_s} - 1\right) \tag{3.3a}$$

$$T_{Ci}\frac{dT_{STi}}{dt} = -T_{STi} + P_{SVi} \tag{3.3b}$$

$$T_{5i}\frac{dT_{Mi}}{dt} = -T_{Mi} + \left(\frac{T_{4i}}{T_{Ci}} - 1\right)T_{STi} \tag{3.3c}$$

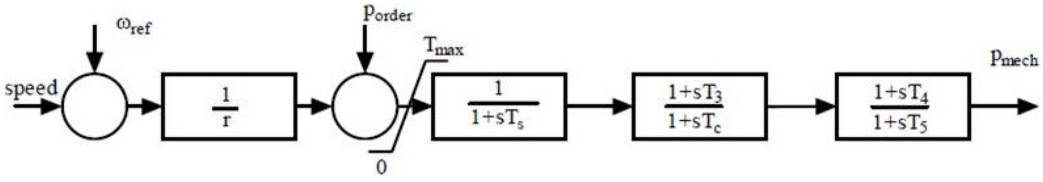

Figure 3.2: Simple turbine governor [17]

$$\begin{aligned} 0 = {} & V_i e^{j\theta i} + (R_{si} + jX'_{di})(I_{di} + jI_{qi})e^{j(\delta_i - \frac{\pi}{2})} \\ & - E'^{o}_i e^{j(\delta_i + \delta'^{o}_i)} \end{aligned} \tag{3.4a}$$

$$\begin{aligned} V_i e^{j\theta i}(I_{di} - jI_{qi})e^{-j(\delta_i - \frac{\pi}{2})} + P_{Li} + jQ_{Li} \\ = \sum_{k=1}^{9} V_i V_k Y_{ik} e^{j(\theta_i - \theta_k - \alpha_{ik})} \end{aligned} \tag{3.4b}$$

$$P_{Li} + jQ_{Li} = \sum_{k=1}^{9} V_i V_k Y_{ik} e^{(j\theta_i - \theta_k - \alpha_{ik})} \tag{3.4c}$$

Note: Equations (3.1)-(3.3), (3.4a), and (3.4b) are for $i = 1, 2, 3$, and equation (3.4c) is for $i = 4, \ldots, 9$.

Using the differential equations given in (3.2) and (3.3), the stator algebraic equations from (3.4a), and the network equations in (3.4b) and (3.4c), the dynamic behavior of the system can be characterized through the application of 15 differential equations and 12 complex algebraic relationships. The state vector of the resulting system is

$$\underline{x} = [\underline{x}_1^T \;\; \underline{x}_2^T \;\; \underline{x}_3^T]^T, \tag{3.5}$$

where

$$\underline{x}_i = [\delta_i \;\; \omega_i \;\; P_{SVi} \;\; T_{STi} \;\; T_{Mi}]^T \qquad i = 1, 2, 3 \tag{3.6}$$

The vector of algebraic variables is

$$\underline{y} = [\underline{I}_{d-q}^T \;\; \underline{V}^T \;\; \underline{\theta}^T]^T, \tag{3.7}$$

where

$$\underline{I}_{d-q} = [I_{d1} \;\; I_{q1} \;\; \ldots \;\; I_{d3} \;\; I_{q3}]^T \tag{3.8a}$$
$$\underline{V} = [V_1 \;\; V_2 \;\; \ldots \;\; V_8 \;\; V_9]^T \tag{3.8b}$$
$$\underline{\theta} = [\theta_1 \;\; \theta_2 \;\; \ldots \;\; \theta_8 \;\; \theta_9]^T. \tag{3.8c}$$

Combining differential equations (3.2) and (3.3), and algebraic equations (3.4b) and (3.4c), the system can be described as a system of non-linear differential-algebraic equations (DAE).

$$\dot{\underline{x}} = \underline{f}\left(\underline{x}, \underline{y}, \underline{u}\right) \tag{3.9a}$$
$$\underline{0} = \underline{g}\left(\underline{x}, \underline{y}\right), \tag{3.9b}$$

where the input vector $\underline{u}$ is given by

$$\underline{u} = [\underline{u}_1^T \;\; \underline{u}_2^T \;\; \underline{u}_3^T]^T \tag{3.10a}$$
$$\underline{u}_i = [\omega_s \;\; P_{Ci}]^T \qquad i = 1, 2, 3 \tag{3.10b}$$

3.1 Transient simulation with the non-linear DAE

A 100 MW constant power load at bus 3 (in area A) is permanently brought online at $t = 1$ s to simulate a fault that disturbs the power balance of the 9-bus system. This disturbs the steady-state operating point shown in Figure 3.1 and the transient response of the system is recorded. The transient response of the generators' frequency ($f_i = w_i/2\pi$) is shown in Figure 3.3. Assuming a threshold of 60±0.005 Hz for detection, there is a finite delay in the drop of the generators' frequency in response to the sudden increase in load at bus 3. Figure 3.4 shows snapshots of a contour of frequency values along the 9-bus system. The frequency at a bus is directly influenced by

the frequency of generators closer to the bus. Only the frequency in area A drops below 59.995 Hz even after 0.4 s of the fault, with very little change in frequency in areas B and C. While the inertias (H_1 and H_2) of the generators in areas B and C resist a change in their speed, the generator in area A loses rotational kinetic energy. This goes towards supplying the extra load, and causes a drop in the frequency of area A. Similarly, frequency in area C has not dropped below 59.995 Hz after 1.0 s of the fault. Frequency in area C decreases by 0.005 Hz only after approximately 1.8 s of the fault. Observing the dynamic states, generator power output, and input torques of this small 9-bus system provides intuition into the electromechanical disturbance prorogation.

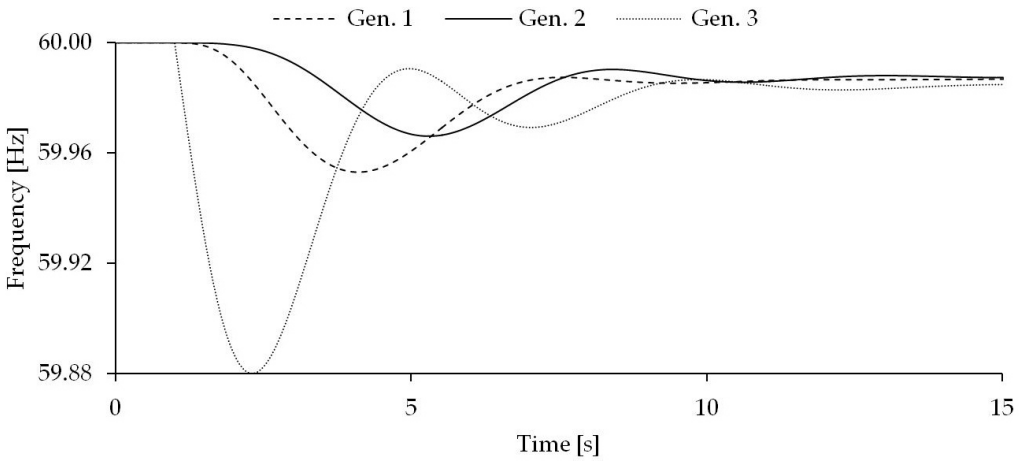

Figure 3.3: Transient response of generator frequency for 9-bus system

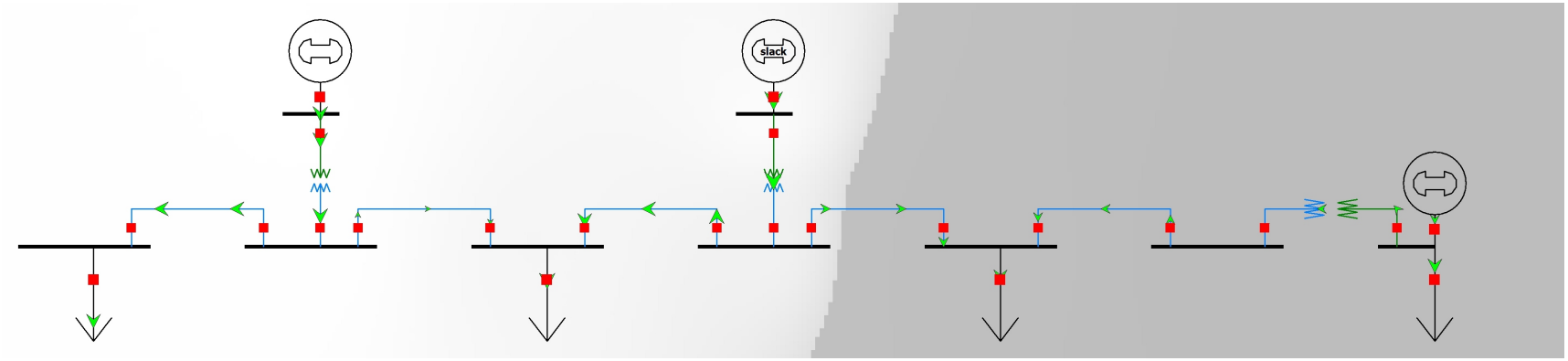

(a) 0.4 s after fault

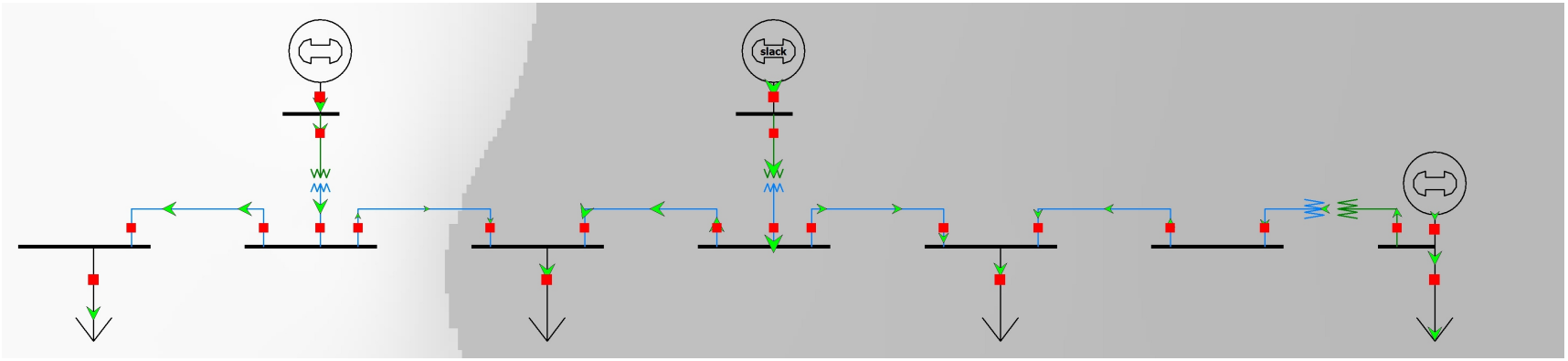

(b) 1.0 s after fault

Figure 3.4: Contour of frequency showing snapshots of disturbance prorogation (white: $f = 60.000$ Hz, dark grey: $f < 59.995$ Hz)

3.2 Simulation with the linearized model

Next, the system model is linearized around its initial operating point as shown in Figure 3.1. Assuming $\underline{u}$ is kept constant, the DAE in (3.9) are linearized with respect to both $\underline{x}$ and $\underline{y}$ to yield

$$\begin{bmatrix} \delta\underline{\dot{x}} \\ \\ \underline{0} \end{bmatrix} = \begin{bmatrix} \frac{\partial \underline{f}}{\partial \underline{x}} & \frac{\partial \underline{f}}{\partial \underline{y}} \\ \\ \frac{\partial \underline{g}}{\partial \underline{x}} & \frac{\partial \underline{g}}{\partial \underline{y}} \end{bmatrix} \begin{bmatrix} \delta\underline{x} \\ \\ \delta\underline{y} \end{bmatrix} = \begin{bmatrix} \underline{A} & \underline{B} \\ \\ \underline{C} & \underline{D} \end{bmatrix} \begin{bmatrix} \delta\underline{x} \\ \\ \delta\underline{y} \end{bmatrix} \tag{3.11}$$

which can be simplified and expressed as

$$\delta\underline{\dot{x}} = \left[\underline{A} - \underline{B}\underline{D}^{-1}\underline{C}\right] \delta\underline{x} = \underline{A}_{sys}\delta\underline{x} \tag{3.12}$$

The eigenvalues of $\underline{A}_{sys}$ are shown in Table 3.1 for the initial operating condition of the 9-bus system, and modes are shown in Table 3.2. These modes are about the same frequency as calculated from the oscillations from Figure 3.3. Also, each mode has been intentionally numbered to correspond to the generator frequency that is most influenced by it; i.e., Mode 1 has the most influence over ω_1. It is interesting to observe how a linearized model responds as compared to the non-linear DAE for the same fault. Similar to equations (3.11) and (3.12), a linearization is carried out for the DAE in (3.9) which yields $\delta\underline{\dot{x}}_{new} = \underline{A}_{new}\delta\underline{x}_{new} + \underline{B}_{new}\delta\underline{u}_{new}$. The input vector, $\underline{u}_{new}$ contains the load at bus 3 which is treated as an input variable. The same fault (as in Section 3.1) is applied to the linearized model by switching in a 100 MW constant power load at bus 3 (in area A) at $t = 1$ s. Once again,

Table 3.1: Eigenvalues of $\underline{A}_{sys}$

-10.1490	-10.2302	-10.2680
$-0.3317 \pm j1.4640$ [2]	$-0.3927 \pm j1.3122$ [3]	-1.3717
$-0.6283 \pm j0.7781$ [1]	-0.9256	-0.4977
0.0000	-0.0676	-0.0847

Table 3.2: Modes of the linearized system

Mode	Frequency [Hz]	Damping ratio
1	0.1238	0.6282
2	0.2330	0.2210
3	0.2088	0.2867

the power balance is disturbed and the transient behavior of the linearized system is recorded.

Figure 3.5 shows a comparison in the transient response of the generators' frequency for the simulation with non-linear DAE versus the simulation with the linearized model. For this particular fault in the 9-bus system, it is observed that the generators' frequency during transient response of the linearized model seems to be slightly lower than the values observed in simulation of non-linear DAE. The motivation for comparing the non-linear DAE and the linearized model is to compare the time delay associated with the propagation of electromechanical disturbance caused by the fault at bus 3 in the 9-bus system. Assuming a threshold of 60±0.005 Hz, the following quantity is defined and calculated. The values are presented in Table 3.3.

$$\begin{aligned} \Delta t_i \triangleq & \text{ Time elapsed from the instance of the fault,} \\ & \text{until } f_i \text{ drops below 59.995 Hz} \\ & i = 1, 2, 3 \end{aligned} \tag{3.13}$$

The plots in Figure 3.5 and the values in Table 3.3 show that the time delays are comparable between the non-linear DAE solution and the linearized solution. The time delays observed in the solution of the linearized model are within ±2.4% of the time delays observed in the non-linear DAE solution. Despite the small difference in the time delays in this study, linearized solutions should not be deemed as a replacement. Non-linear solutions are curucial for power system analyses as they provide a more detailed and accurate representation.

Table 3.3: Time delays

	Non-linear DAE	Linearized model
Δt_3 [s]	0.0335	0.0343
Δt_1 [s]	0.8705	0.8653
Δt_2 [s]	1.7750	1.7402

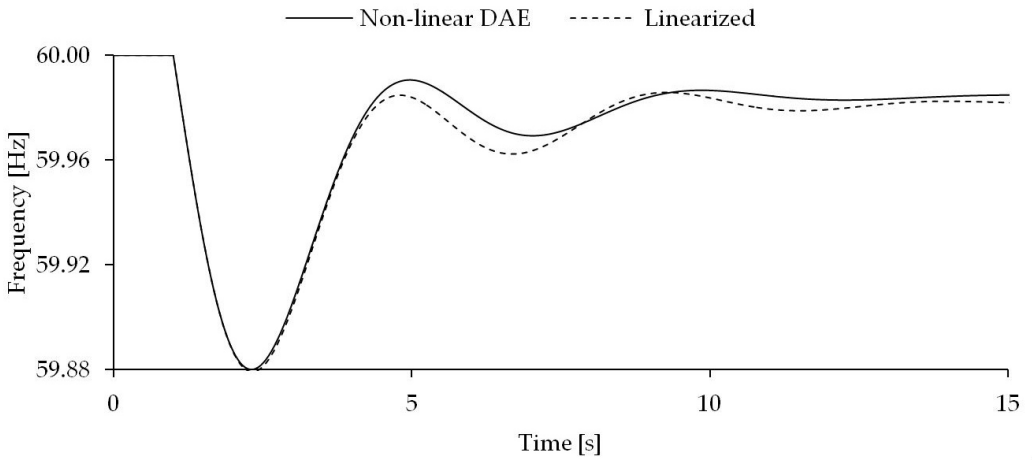

(a) Transient response of generator 3 (in area A) frequency

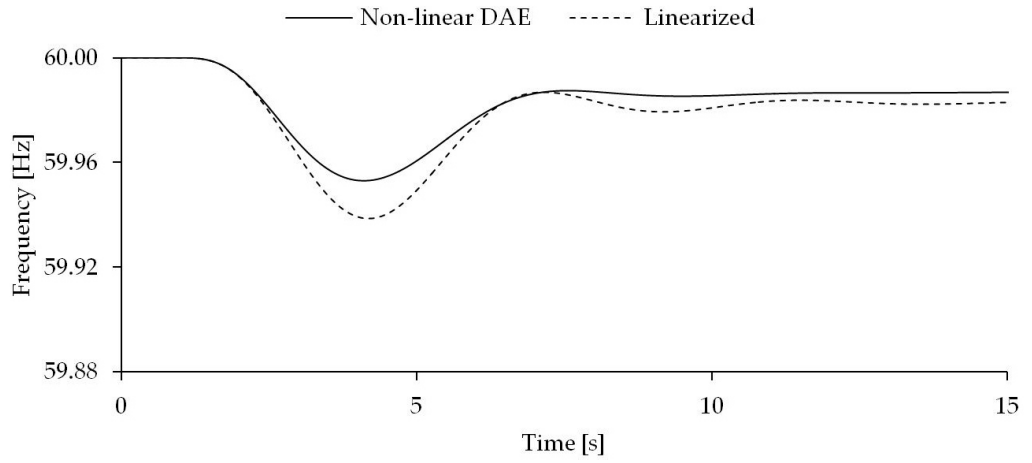

(b) Transient response of generator 1 (in area B) frequency

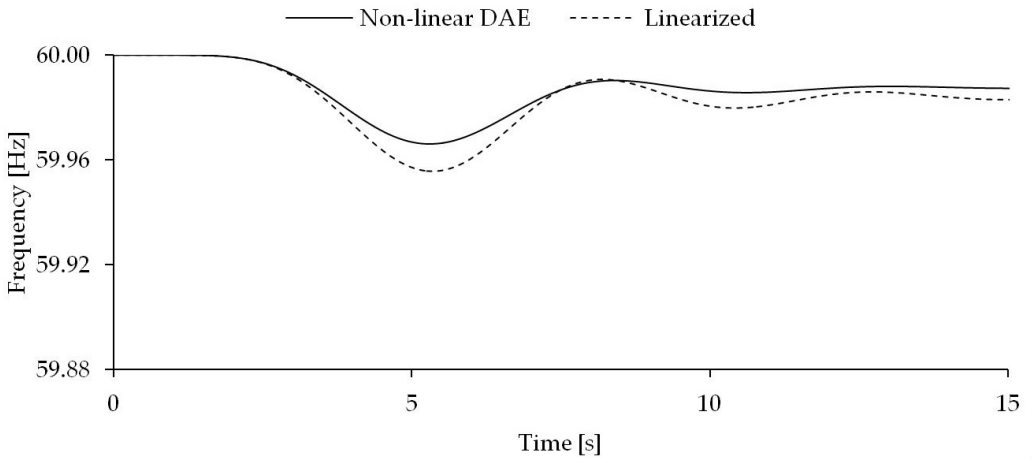

(c) Transient response of generator 2 (in area C) frequency

Figure 3.5: Comparison between the non-linear DAE and the linearized model

CHAPTER 4

UTILITY-SCALE ENERGY STORAGE FOR THE ELECTRIC GRID

4.1 Energy storage devices

Renewable energy resources such as wind and solar are intermittent and unpredictable. To reduce the impact on the grid due to the fluctuations in their generation levels, storage is an essential component to allow the penetration of renewables. This will be even more essential as installed capacity of renewables increases and balancing by conventional power plants will be insufficient to make up for fluctuations in renewable generation. The design of renewable plants with storage will allow renewable plants to be more predictable in their generation. The use of energy storage devices can also provide some capability towards primary frequency response. Of course, proper control and coordination will be required to allow these energy storage devices to add to the governor response of conventional plants in the event of power imbalances.

Technologies for utility-scale electric energy storage have been around for several decades. However the scale of storage is still rather limited. This is one of the most limiting factors of the electric grid. If the pumps for a water circulation system were to momentarily stop working, there would still be the remnant water in the pipes, which will continue flowing, and the pumps have a greater time horizon to restart (as compared to the electric grid). Over short periods of time (i.e. one minute to tens of minutes) there might be no apparent difference felt at various parts of the water circulation network. However, the electric grid maintains a tight balance between load and generation at all instances in time. Not considering the presence of storage, the electricity being consumed at residences or industries is literally created only seconds before it is consumed. The scale of energy/power being delivered is tremendous compared to capacity provided by most conventional

Storage Technology	Main Advantage (Relative)	Disadvantage (Relative)	Power Application	Energy Application
High-speed Flywheels (FW)	High Power	Low Energy Density	●	
Electrochemical Capacitors (EC)	Long Cycle Life	Very Low Energy Density	●	
Traditional Lead Acid (TLA)	Low Capital Cost	Limited Cycle Life	●	○
Advanced LA with Carbon Enhanced Electrodes (ALA-CEE)	Low Capital Cost	Low Energy Density	●	●
Sodium Sulfur (Na/S)	High Power and Energy Density	Cost and Needs to Run at High Temperatures	●	●
Lithium-ion (Li-ion)	High Power and Energy Density	Cost and Increased Control Circuit Needs	●	◐
Zinc Bromine (Zn/Br)	Independent Power and Energy	Medium Energy Density	◐	●
Vanadium Redox (VRB)	Independent Power and Energy	Medium Energy Density	◐	●
Compressed Air Energy Storage (CAES)	High Energy, Low Cost	Special Site Requirements		●
Pumped Hydro (PH)	High Energy, Low Cost	Special Site Requirements		●

● Fully capable and reasonable ◐ Reasonable for this application ○ Feasible but not quite practical or economical NONE Not feasible or economical

Figure 4.1: List of energy storage technologies [18]

storage means within economic limitations.

Figure 4.1 shows some energy storage technologies. Broadly, they can be divided into two categories: (i) Power applications, and (ii) Energy applications. Devices such as flywheels, capacitors, and traditional lead-acid batteries can provide pulses of energy. They are useful in fast frequency regulation in the electric grid and have been used widely. However, these devices cannot store much energy due to economic, size, or chemical limitations. Therefore they are only useful in providing energy for short durations of time.

The other class of storage units is more suited towards longer-term energy storage such as a day or up to a week. The residual drain/discharge from most of these devices makes it uneconomical to even attempt storage for anything beyond a few days. Such technologies include flow batteries, pumped hydro, sodium-sulfur batteries, and compressed air energy storage. These technologies can have different scopes of implementation depending on advantages or disadvantages attached to each of them as summarized in Figure 4.1.

The amount of energy storage in the grid today is minuscule compared to the transactions that occur between entities or between geographic regions.

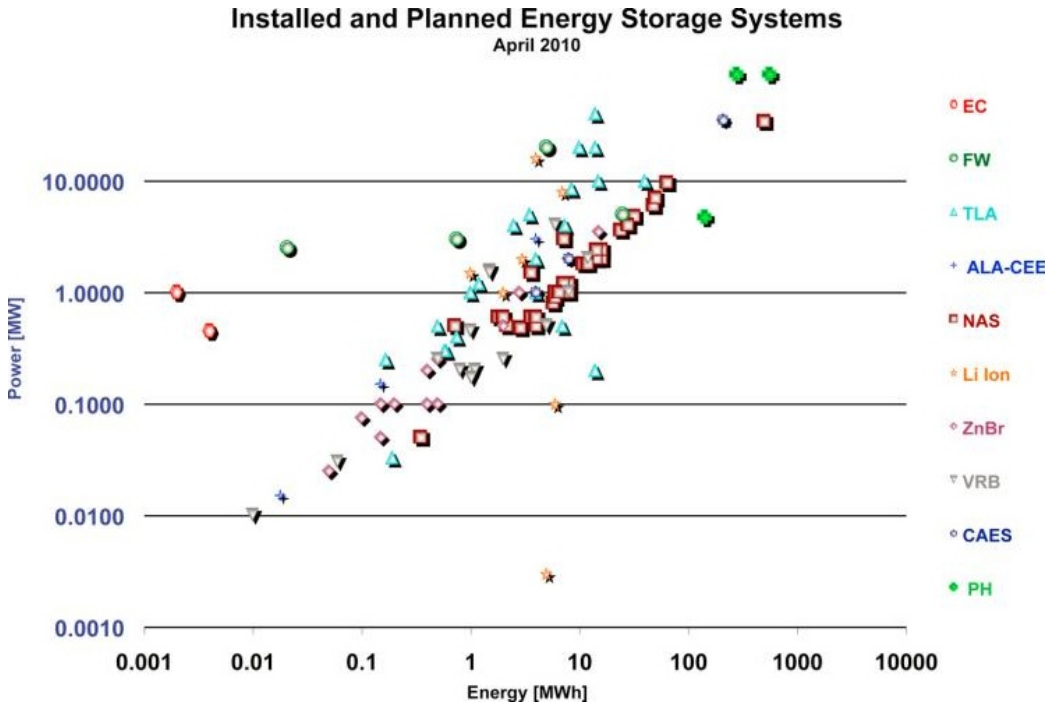

Figure 4.2: Installed and planned energy storage systems [18]

Most storage is used for fast frequency regulation to maintain a good frequency quality for consumers. The desired direction of growth in this sector is towards units that can store large quantities of energy and also be brought online or ramped up/down relatively fast so that they can respond to changing grid conditions. Figure 4.2 shows such systems, which have been installed and planned. It seems pumped hydro, compressed air energy storage, and sodium-sulfur batteries are the ones that are (or predicted to be) the most successful in being suitable for both energy and power applications. However, it is important to note that both pumped hydro and compressed air energy storage require large amounts of space - they cannot be built in every location. This leaves sodium sulfur batteries as a viable solution in terms of having no geographic constraints, yet being able to meet high power and energy ratios. There is a push towards larger energy storage systems that can be utilized at the grid-scale due to the increasing penetration of intermittent renewable generation sources. This will allow the amount of grid-scale energy storage to be commensurate with the required level of primary frequency response so as to respond to power imbalances in the electric grid.

4.2 Cost considerations

The various technologies discussed in the previous section are at different price points. The material used, cost of production, scalability, and growth potential all have an influence over their price. Figure 4.3 shows a spread of technologies with their respective energy density and cost. Once again sodium-sulfur batteries seem to be a viable option along with lithium-ion batteries.

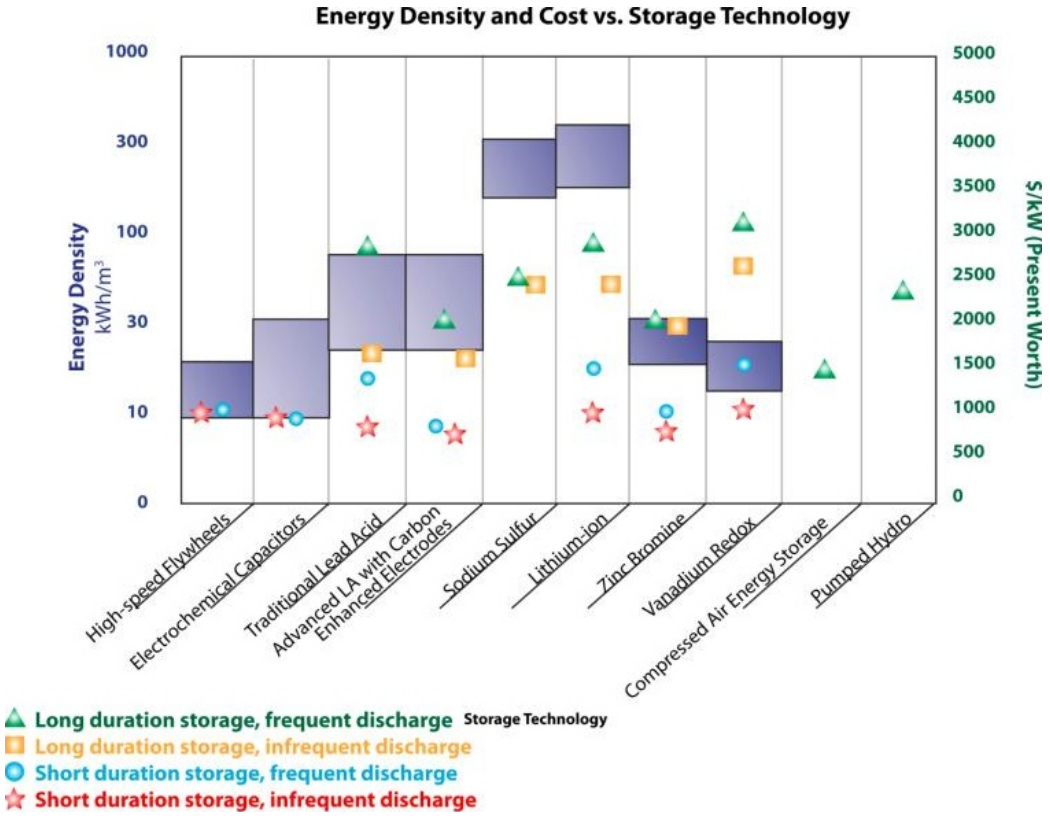

Figure 4.3: Energy density and cost vs. storage technologies [18]

4.3 Storage location on the electric grid

The electric grid consists of various voltage levels. Transmission voltage levels are higher than distribution voltage levels, which allows transmission of bulk power. If an energy storage unit is to be installed to mitigate intermittency from a wind farm, it is best if it is kept as close to the wind farm as possible. On a system level, this will enable the wind farm to be perceived

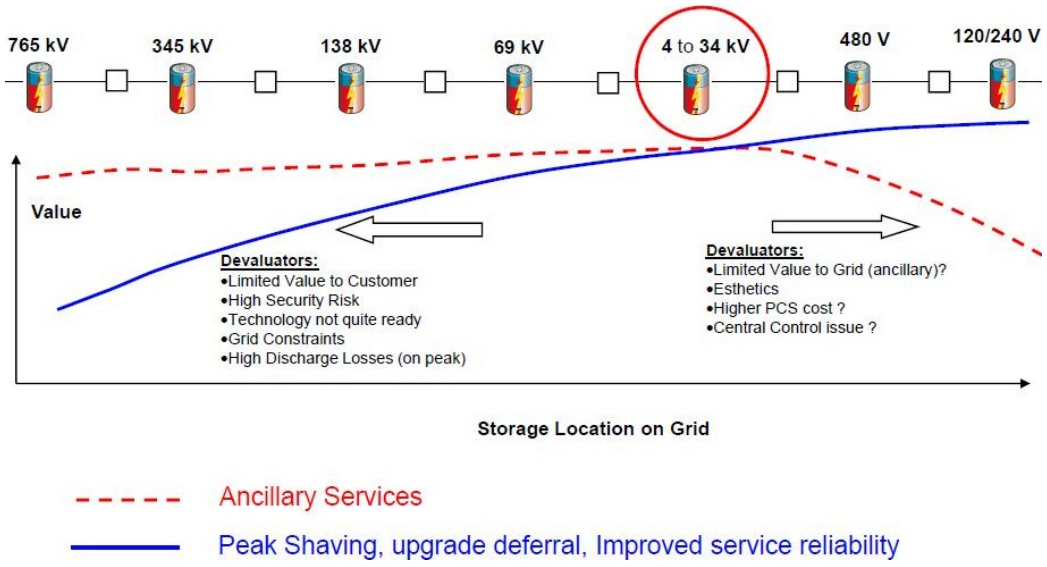

Figure 4.4: Value of energy storage at different voltage levels [18]

like a conventional power plant (except for the much lower inertia) There is no doubt that studies need to be performed to decide on the size of storage capacity and control schemes. However, studies by the Electricity Storage Association [18] recommend that if storage units are being installed for ancillary services and peak shaving, then their best location is at the 4 kV to 34

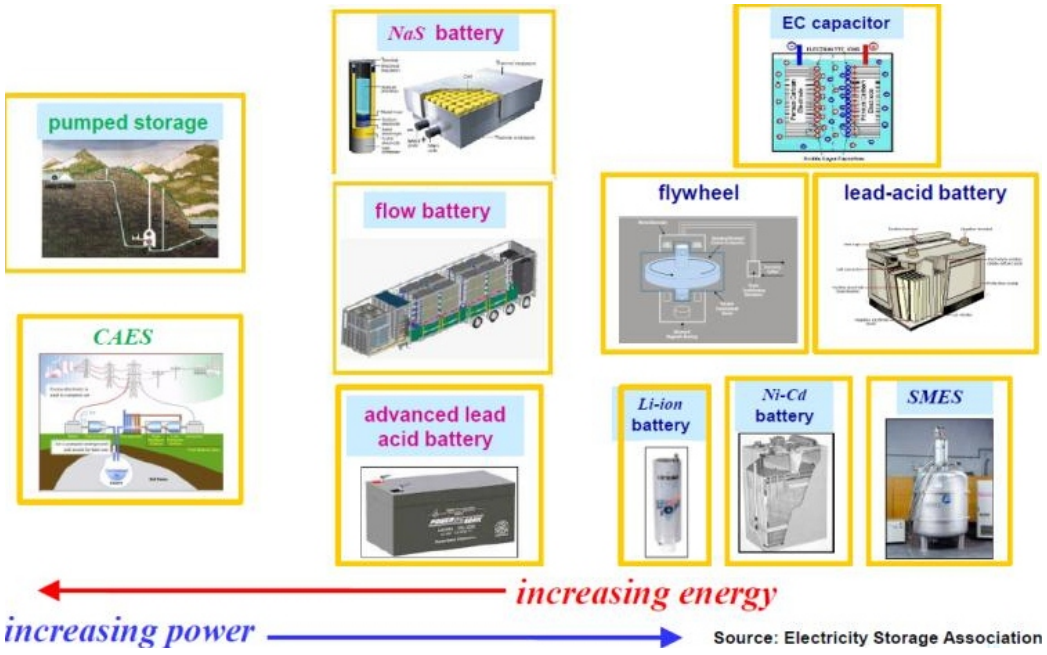

Figure 4.5: Energy storage options in relation to energy and power [18]

kV voltage levels (Figure 4.4). This will allow the distribution side to yield benefits equal to the transmission side. This scheme might be somewhat optimal from the perspective of ancillary services and peak shaving. However, this may not be equally beneficial if the purpose of this storage unit is to provide primary frequency response for the wind farm and make it appear almost like a conventional power plant.

Figure 4.5 shows various storage technologies. The key take-away is that they usually do not meet both power and energy requirements. Increasing power and increasing energy are usually conflicting decision variables while choosing an energy storage system. The electric grid is evolving. To allow for a greater penetration of intermittent renewables, grid-scale energy storage will be required. The solution however will depend largely on the type of intermittency being mitigated, the service being provided, the existing power system network, and economic and security (both power system security and infrastructure security) considerations.

CHAPTER 5

USING SMART DEVICES TO PROVIDE DISTRIBUTED REACTIVE POWER SUPPORT

There has been an increasing mention of smart devices being utilized for active demand-side management. This covers a variety of strategies such as active response of home appliances, HVAC systems, hybrid electric vehicles (HEVs), uninterrupted power supplies (UPSs), and even solar arrays. A smart device has the ability to communicate with the smart grid. The presence of digital processors and sensors provide them the ability to move beyond localized control schemes and respond to systemwide objectives through remote communication and algorithms. This chapter outlines part of the ongoing research to provide an authenticated framework for mobilizing distribution-level devices to provide reactive power support. More specifically, it discusses the facilitation of reactive power injection control at the residential-level.

While the advantages of distributed voltage support have been shown for decades, the use of power electronics in the power systems industry is more modern, becoming prominent in the 21st century. Traditionally, reactive power support was implemented by switching large banks of capacitors. SVCs have been used since the '70s, but it wasn't until the late '90s that power electronics started to gain traction for active switching applications. In 1997 the acronym FACTS was added to the IEEE dictionary and the first STATCOM was installed in 1999 [19]. The most effective solution for a load that is consuming reactive power is power factor correction or compensation at the source. The Smart Grid opens up the opportunity for a level of distributed voltage support that has not been used in the past.

Figure 5.1 shows possible constituents of a reactive support group [20]. As seen in the diagram, the plug-in HEV (PHEV) is a smart device which can be remotely controlled by a manager higher up in the hierarchy of the distribution/transmission network. These devices would be scattered over a large area and require substation-level co-ordinated aggregate control to meet

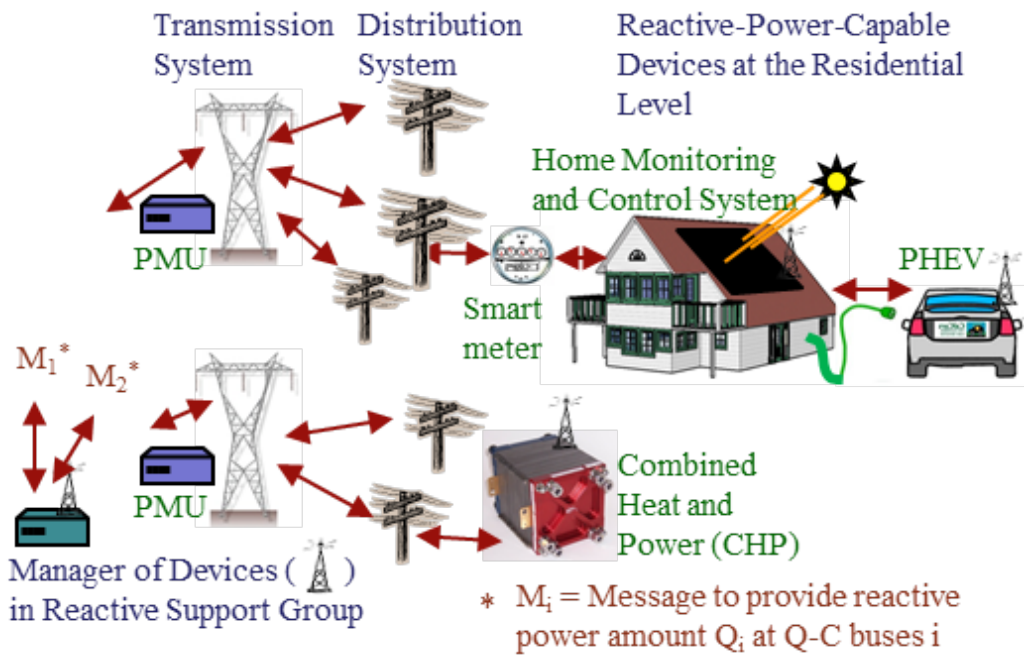

Figure 5.1: Constituents of a reactive power support group [18]

multiple objectives such as voltage set points, minimization in transmission line loading, or minimization of network losses. At present, such devices are not common and remote control network algorithms are still a major research area. In theory such control schemes can be implemented with concurrent development of secure communication and smart device technology. The remainder of this chapter is organized as follows. Section 5.1 presents examples to motivate the idea of reactive power-based voltage regulation in a distribution network. Section 5.2 discusses areas of possible application.

5.1 Reactive power voltage support

5.1.1 Traditional use of shunt capacitor banks

Figure 5.2 shows a one-line diagram of a primary feeder supplying power to a load at the end of the feeder [21]. The load bus has a shunt of $-j2.10$ p.u. which can be switched in or out. The sending end voltage, V_S, is maintained at 1.05 p.u. Summary of calculations for the cases when the shunt is disconnected and when connected is shown in Table 5.1.

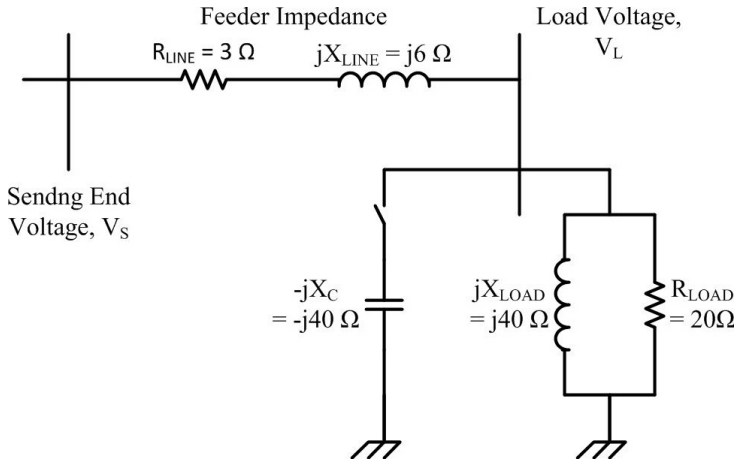

Figure 5.2: Shunt capacitor (switched out) at the end of a primary feeder ($S_{base3\phi} = 10$ and $V_{baseLL} = 13.8$ kV)

Table 5.1: Summary of calculations

	Shunt disconnected	Shunt connected
Line current, $\|I_{LINE}\|$ [p.u.]	0.8473	0.8414
Load voltage, $\|V_L\|$ [p.u.]	0.7957	0.8833
Real power loss, $\|P_{LOSS}\|$ [p.u.]	0.1131	0.1115

Since the transmission of reactive power over long distances (from power plants to loads) is not economically feasible, shunt capacitors are widely used in distribution systems. The example in Figure 5.2 shows the benefit of having reactive power injection closer to the load bus. When the shunt capacitor bank is connected, $|I_{LINE}|$, decreases, $|V_L|$ increases, and $|P_{LOSS}|$ decreases (Table 5.1). All of the above are desirable effects which can be achieved by power factor correction at the load bus instead of reactive power being supplied from the distribution substation.

Although the above example results in unity power factor at the load bus, similar effects can be achieved through real-time control of smart devices which help push the power factor closer to unity. Unlike the shunt capacitor bank, these smart devices will be able to inject reactive power in a more distributed way. This will be particularly helpful in residential distribution networks which are typically radial and are prone to under-voltage conditions.

5.1.2 Proposed use of smart devices as variable reactive power sources

In order to demonstrate the feasibility of distributed smart devices to provide reactive power, the modified 44-bus (originally 37-bus [22]) power system illustrated in Figure 5.3 is simulated using PowerWorld Simulator 16. It has been adapted to include load buses in a radial configuration at the bus named WOLEN69. In essence, this reflects additional detail in the network topology as shown in Figure 5.4. Usually, such detail is ignored for large system studies. However, studying this extended network helps enforce the idea of distributed reactive voltage support.

Table 5.2: Bus voltage magnitudes for WOLEN69 subnetwork

Bus voltages [p.u.]	Only shunt capacitor is connected at WOLEN69	Only distributed smart devices are connected
WOLEN69	1.0063	1.0063
W69	0.9632	0.9822
W69_1	0.9580	0.9783
W69_1_1	0.9563	0.9771

Distributed devices make it possible to inject reactive power more evenly along the radial load buses. These distributed injections ensure a better power factor at each load bus, ultimately resulting in a more even voltage profile throughout the radial network (Table 5.2). Widespread presence of such smart devices would reduce the demand for reactive power, allowing generators to operate within the same ratings while increasing real power production. Such benefits make distributed reactive voltage support appealing.

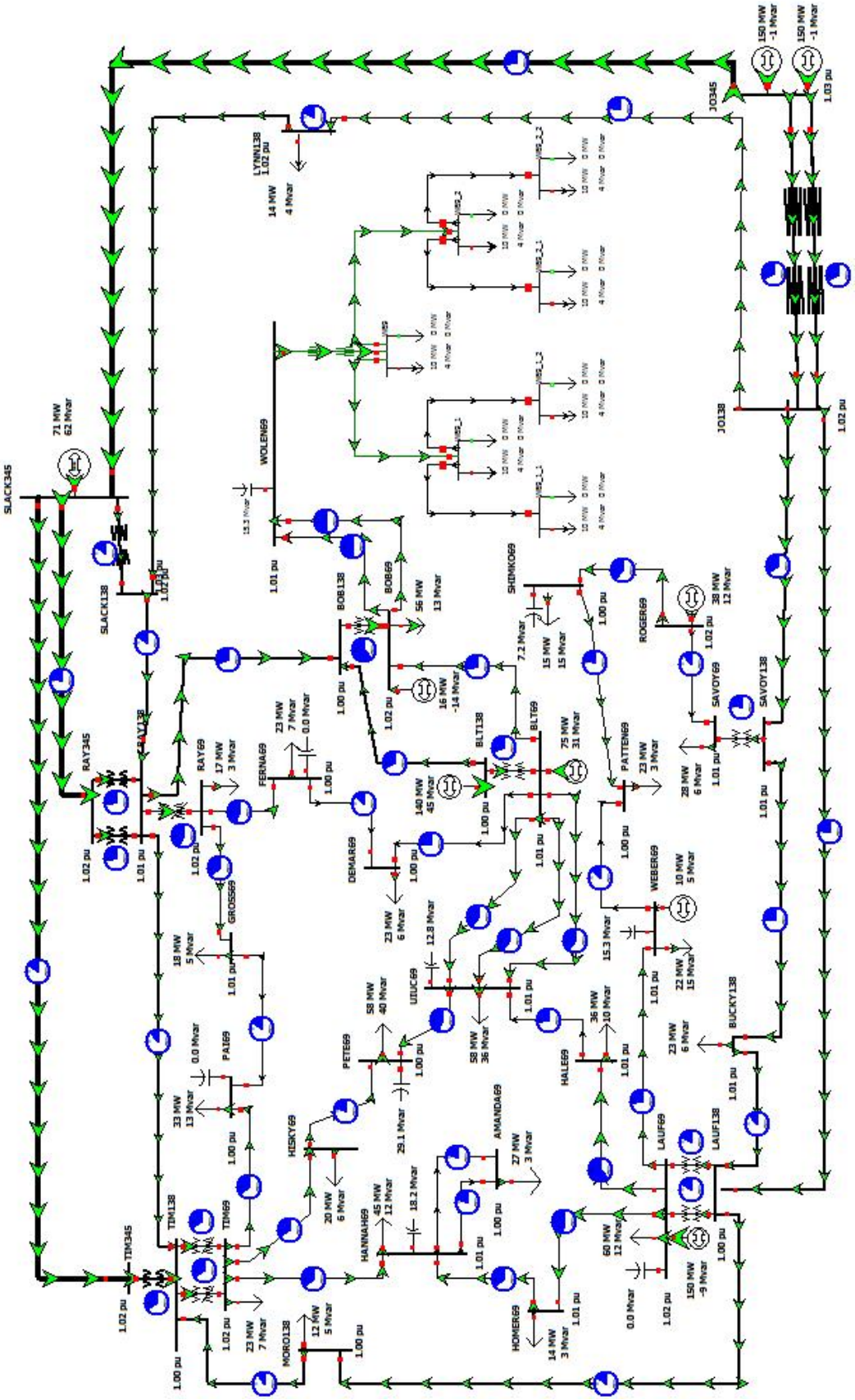

Figure 5.3: Modified 44-bus network (originally 37-bus)

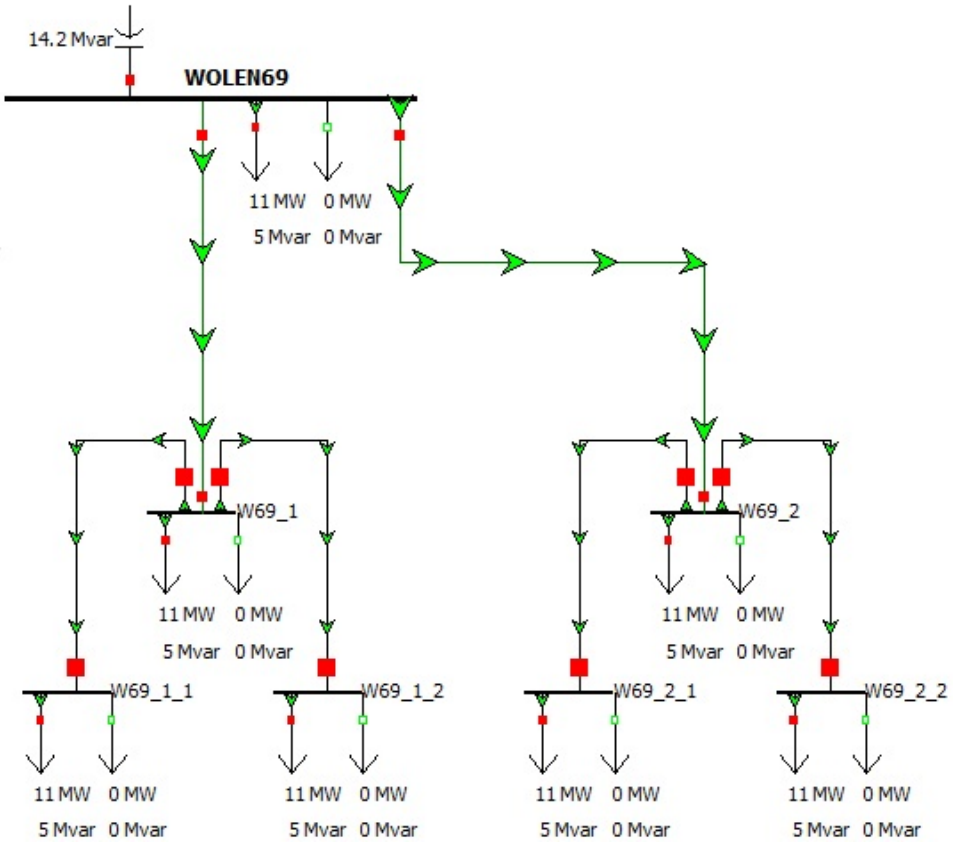

Figure 5.4: 13.8 kV subnetwork of WOLEN69 (shunt capacitor is connected and smart devices are disconnected)

5.2 Applications

With the advent of the Smart Grid to the average household, comes opportunity to improve the nation's grid on many different levels. The impact of EV and PHEVs on the grid is an active area of research. Typically, a vehicle can be charged overnight when the demand for electricity is low. To improve the overall efficiency of transmission, the power factor at which the vehicle is charged can be controlled. Furthermore, this method can be used to provide reactive voltage support when the car battery is at full charge, even to provide the option of real power support in the case of a critical need, or to provide backup power during an outage. A multitude of other similar devices can be used as well. The research presented in this chapter focuses on EV/PHEVs, PV systems, and UPS devices. The motivation lies in the improvements that can be made to the nation's grid through the use of existing products.

Table 5.3: Charging level specifications

	Voltage [V]	Phase	Peak current [A]
ac level 1	120	Single-phase	16
ac level 2	240	Split-phase	32

The advantages of injecting reactive power locally are clear from the discussion in Section 5.1. By improving the power factor, the line current is reduced, hence reducing the line losses. However, the benefits need to be weighed against the drawbacks. The maximum charge current typically depends on the charging method available. The assumption for this research is based on a consumer grade system from [23, 24], so levels 1 and 2 charging as shown in Table 5.3 are considered. By charging at a non-unity power factor the charge time will be extended. Furthermore, the losses in the charging system will increase and the stress on the electrical components will be slightly higher. Ultimately the decision to choose should be left to the consumer based on the incentives. That being said, the focus of this research does not include power system economics, pricing, or the communication framework required. Agent-based technologies could be a good choice as presented in [25, 26]. Further research is being conducted on the effects of malicious attacks relating to the distributed injection of reactive power.

Another point to consider is the availability of these devices since the peak-load occurs during the day. Solar panels and UPS systems are stationary, but PHEVs may be out on the road, at home, or at work. It is reasonable to assume that the number of cars in an area will have a correlation with the number of people and ultimately the load in that area. If charge stations are made available in the future, PHEVs can have a greater impact by participating in these areas that are expected to have a higher load. The modes of operation of interest (1, 2, and 3) are labeled in Figure 5.5; consuming reactive power is not being considered. Option 1 is the base scenario – charging at a unity power factor with no reactive power injection. Option 2 shows charging at a leading power factor. Both the current magnitude and current angle can be adjusted. A slow charge is recommended when time is not critical, such as overnight charging. Since the magnitude of current is smaller, the stress on the batteries/system as well as conduction losses are reduced. Option 3 is used to solely inject reactive power while the loss in the

system is to be compensated by the grid.

Although the supply of real power is a possibility, it is assumed to be undesirable and such modes of operation will not be used [27, 28]. The objective is to supply reactive power strictly from the available capacitance (i.e. stored charge), without affecting battery life. As such, the chemistry of the cells is not critical, but proper battery management systems must be used to protect against improper use. For initial experiments, $LiFePO_4$ batteries have been selected based on considerations such as safety and power density. The dc bus voltage is application specific; for this project, it was selected to be 330 V based on the inverter used [29]. As always, there is a trade-off in using a higher voltage to achieve less conduction losses versus increased switching losses.

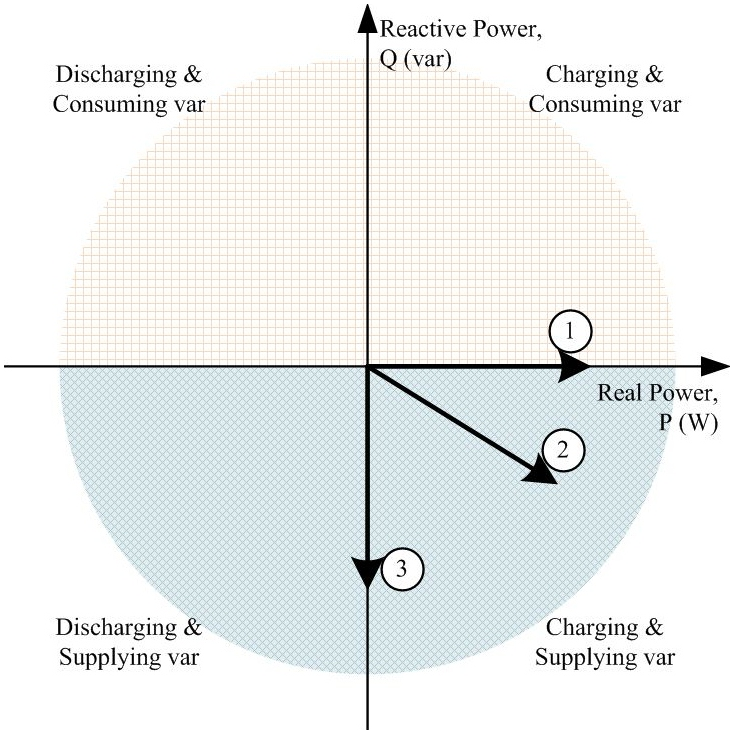

Figure 5.5: Modes of operation (load notation: $P_L + jQ_L$)

CHAPTER 6

BATTERY-INVERTER DEVICE SIMULATION

This chapter presents a method of controlling a single smart device purely for the intended purpose of reactive power injection. The presence of suitable power electronics, sensors, and a digital processor in many modern devices makes them suitable for similar purposes. For example, the reader can imagine a PHEV set up to inject reactive power. To show the basic scheme, a simple battery-inverter device is simulated in Simulink.

6.1 Simulation setup

Figure 6.1 shows the Simulink block diagram. The model for the battery type is Li-ion with parameters similar to a batery pack consisting of approximately 100 series-connected $LiFePO_4$ batteries. Such batteries are being used in energy storage systems and HEVs [30]. As seen in Figure 6.1, the battery (330 V) is connected in parallel with a dc bus capacitor and to an H-bridge. The bridge is operated as an inverter and the output of the H-bridge is connected to a 120 V ac wall outlet.

The remaining blocks form a current controlled hysteresis loop. This requires a voltage sensor to detect the wall outlet voltage-phase and a current sensor to monitor the injected current. In the simulation, the commanded current is set to 10 A ac. The simulation shows that such a setup is able to track the voltage and inject a current which is almost $\frac{\pi}{2}$ rad out of phase. This translates to an injection of reactive power except for the system's real power losses being compensated from the grid. In this case, the power factor of this device would be approaching 0 leading with respect to the grid.

In Figure 6.2, parameters such as battery characteristics and value of C_1 have been adjusted to be as close of a match to the actual hardware which will be used to implement this scheme. The hysteresis bounds and values

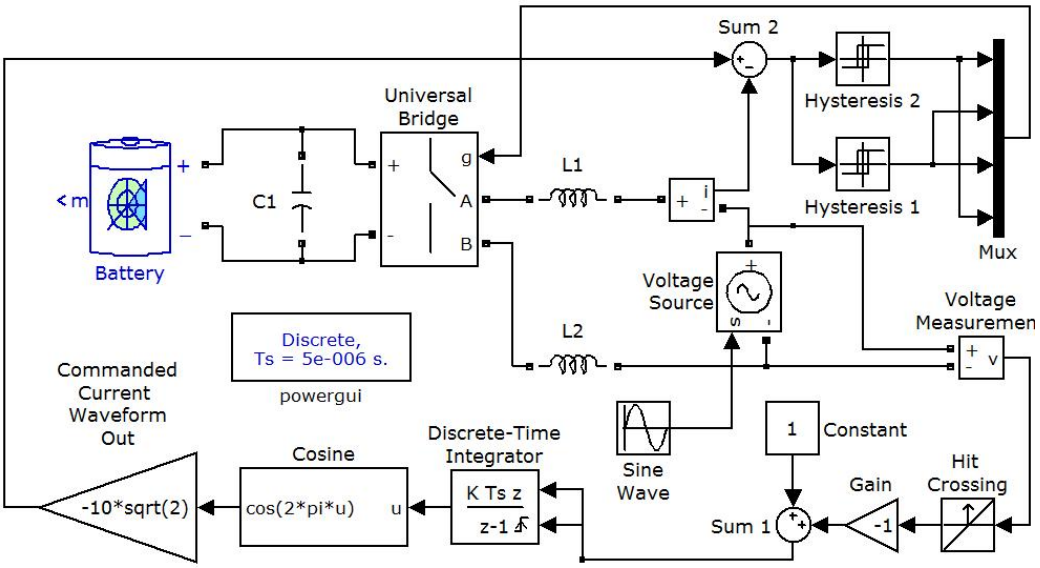

Figure 6.1: Simulink block diagram of the battery-inverter device

of L_1 and L_2 have also been tweaked to ensure that the switching frequency remains within the capability of the hardware.

The simulation shows that this control scheme is able to detect the zero-crossing of the wall voltage, V_{WALL} (Figure 6.2(a)) and command an injected current which is $\frac{\pi}{2}$ rad lagging (equivalent to commanding a drawn current which is $\frac{\pi}{2}$ rad leading) with respect to V_{WALL}. The hysteresis loop is able to track the commanded current and ensure that the injected current, $I_{INJECTED}$, stays within limits of the hysteresis loop. As seen in Figure 6.2(b), $I_{INJECTED}$ has significant harmonic content and would not be recommended for grid interfacing. A solution for reducing harmonic content will be addressed during hardware implementation and is discussed in Section 6.2. At $t = 0$ s (Figure 6.2), a command is issued to inject 10 A ac. The assumption is that the dc link capacitor, C_1, is fully charged before $t = 0$ s. Figure 6.2(c) shows that the battery-inverter device initially draws real power as the value of $P_{INJECTED}$ reaches approximately -300 W. After approximately one cycle, it reaches a steady-state value of -23 W, corresponding to system losses. Since the simulation model has bidirectional current flow capability, the battery remains fully charged throughout. This is a desirable scheme that can be incorporated into a charger of a PHEV [27]. The injected reactive power, $Q_{INJECTED}$, increases to its steady-state value of about 1.2 kvar in the same duration.

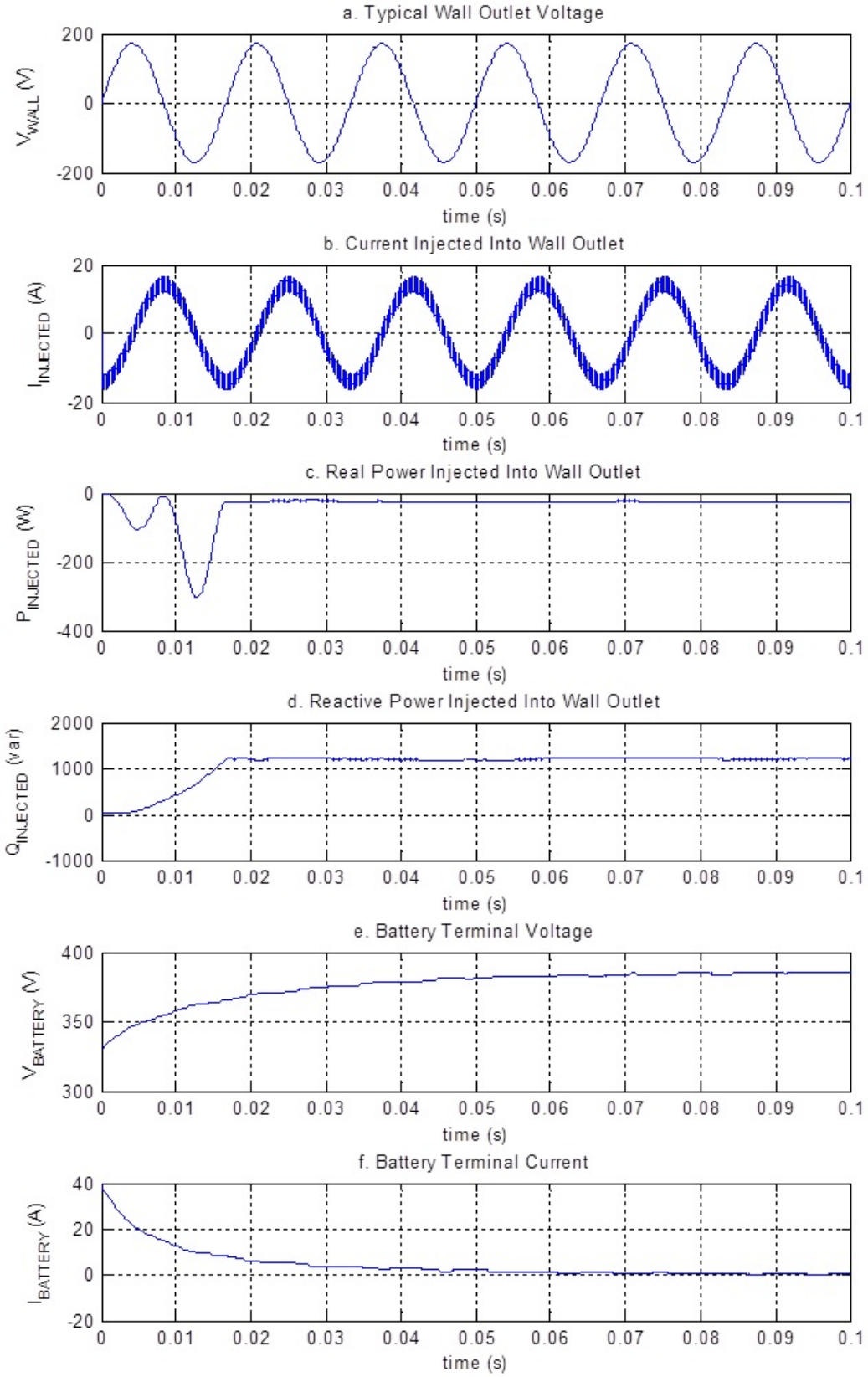

Figure 6.2: Battery-inverter device simulation results (injected notation)

6.2 Discussion

Figure 6.2(e, f) show the voltage, $V_{BATTERY}$, and current drawn, $I_{BATTERY}$, at the battery terminals. Studying these signals is necessary to understand what kind of voltage and current waveforms the battery will be exposed to. As shown in Figure 6.2(e), the bidirectional nature of the simulation allows the battery to charge up to its maximum rating of about 384 V. In the simulation, this maximum bound is set in the parameters. However, a battery management system would be required to ensure charge and other battery limits in a real hardware implementation. Research on bidirectional supplies such as [27], demonstrate the modes of interest without any adverse effects on the battery.

In the event that regulations might disallow the bidirectional flow of current, the battery will be unable to be charged simultaneously. As the battery discharges, its use will be time-limited. The charge and discharge times will be further studied with an experimental setup in the future. The quick response of the battery-inverter device makes it an attractive candidate for responding to emergency conditions in the electric grid. This battery-inverter is representative of increasing types of upcoming devices. With a proper control framework, such devices can collectively provide voltage support rather than just burdening the grid.

The value of 1.2 kvar was an arbitrary choice of a relatively small value which could be tested in a laboratory setting. Actual capacity would be device dependent. As discussed, $I_{INJECTED}$ shown in Figure 6.2(b) has harmonic content. To work around these unwanted harmonics, a layer of PWM control can be implemented [12] in addition to the current control scheme presented in this chapter.

CHAPTER 7

CONCLUSION AND FUTURE WORK

The North American electric grid is evolving due to the constant need for change so as to alleviate the pressure being felt by aging power systems. Policies are driving the integration of renewable energy sources, and new technologies such as the EV and other residential-level devices have the aggregate capability to impact the technical characteristics of the electric grid. The development of energy storage at the utility-scale is also ramping up very fast. The combined effect of these factors is very likely to alter the technical characteristics and the dynamic system behavior of power systems. This thesis has covered background, historical trends, some of those changes at the system-level, and the possible effects in the near future.

Studying the 9-bus case has allowed for systematic analysis and clear visualization of the electromechanical disturbance propagation phenomenon. Generally, this phenomenon is observed in large-scale interconnected power systems like the Western Interconnection. However, one of the key outcomes of this thesis is the relatively much smaller 9-bus system in Figure 3.1, which is also able to show this phenomenon. Classical machine models and simple turbine-governor models to represent system dynamics, and the non-linear DAE consists of 15 dynamic states and 24 algebraic states. For this 9-bus case, the transient responses of both the non-linear DAE in (3.9) and the linearized model are similar. Also, the time delays observed in the solution of the linearized model are within $\pm 2.4\%$ of the time delays observed in the non-linear DAE solution. The energy storage technologies discussed in this thesis will be able to help the grid from a steady-state perspective but the dynamics of power systems will be changed, and there is a need to develop new tools to interpret system-level and wide-area dynamic behavior.s There is motivation to continue pursuing research ideas to find solutions to the issues mentioned in Section 2.1. Future work is expected to include extensions of the analysis presented in Chapters 2 and 3. Also, the inclusion of mea-

surement data to enhance analysis techniques is planned. A possible area of research would be to explore ways to take advantage of the time delays associated with electromechanical disturbance propagation.

The constant addition of new technology is a sign of progress in the field of power and energy systems. However, many new devices also tend to burden the grid with additional real power demand. The possibility of using smart devices for distributed reactive voltage support is discussed in Chapters 5 and 6. It is a way through which residential-level devices can aggregately be utilized to provide system-level benefits for the electric grid. The sensing and processing required is within the capability of target systems and in many cases, devices could continue operating normally without inconveniencing the user. This presents new possibilities to supply reactive power, both during active and standby modes. Although several control schemes can be remotely implemented, communication, security and consumer confidence still remain a challenge. Cost and robustness of such energy storage and auxiliary technologies would be a major driver in the consumer's willingness to opt in or out of such schemes. Distributed voltage support has the potential to transform the electric grid, empowering the industry to expand its capability of emergency response measures for maintaining stability.

In conclusion, the changes occurring in the North American electric grid will continually alter the norms of system planning, dynamics, and control of power and energy systems. The areas of research discussed in this thesis will grow in parallel to the form bridges between past knowledge and future paradigms.

REFERENCES

[1] Wikipedia commons. (2012, Apr 7). *North American Regional Reliability Councils and Interconnections* [Online]. Available: `http://upload.wikimedia.org/wikipedia/commons/f/f4/NERC-map-en.svg`

[2] Nova Science Now. (2011, Feb 1). Smart Grid [Online]. Available: `http://www.pbs.org/wgbh/nova/tech/power-grid.html`

[3] C. Byrne. (2011, Feb 1). How secure is the smart grid? [Online]. Available: `http://venturebeat.com/2011/02/01/how-secure-is-the-smart-grid/`

[4] M.A. Hanley, Frequency Instability Problems in North American Interconnections, DOE/NETL, Rep. DOE/NETL-2011/1473, May 1, 2011.

[5] North-American Electricity Reliability Council. (2012, Apr 7). Frequency Excursions (Low) [Online]. Available: `http://www.nerc.com/page.php?cid=4|37|257|270`

[6] North-American Electricity Reliability Council. (2012, Apr 7). Frequency Excursions (High) [Online]. Available: `http://www.nerc.com/page.php?cid=4|37|257|270|271`

[7] J.W. Ingleson, E. Allen, "Tracking the Eastern Interconnection frequency governing characteristic," *2010 IEEE Power and Energy Society General Meeting*, pp. 1-6, 25-29 July 2010.

[8] J.S. Thorp et al., "Electromechanical wave propagation in large electric power systems," *IEEE Transactions on Circuits and Systems I: Fundamental Theory and Applications*, vol. 45, pp. 614-622, June 1998.

[9] M.Parashar et al.,"Continuum modeling of electromechanical dynamics in large-scale power systems," IEEE *Transactions on Circuits and Systems I: Regular Papers*, vol. 51, pp. 1848-1858, September 2004.

[10] S. Backhaus, "Propagation Velocity and Damping of a Frequency Disturbance," unpublished.

[11] A.J. Arana et al., "Estimating speed of frequency disturbance propagation through transmission and distribution systems," *2006 IEEE PES Power Systems Conference and Exposition*, pp. 1286-1290.

[12] Western Electricity Coordinating Council. (2011, Sep 22). Executive Summary 2011 WECC 10-Year Regional Transmission Plan [Online]. Available: `http://www.wecc.biz/library/StudyReport/Documents/ExecutiveSummary_Brochure.pdf`

[13] Wikipedia commons. (2012, Apr 7). Brazos Wind Farm [Online]. Available: `http://upload.wikimedia.org/wikipedia/commons/8/8b/GreenMountainWindFarm_Fluvanna_2004.jpg`

[14] National Public Radio. (2011, Sep 26). Visualizing the U.S. Electric Grid [Online]. Available: `http://www.npr.org/templates/story/story.php?storyId=110997398`

[15] Wikipedia commons. (2012, Apr 7). Nellis Solar Plant [Online]. Available: `http://upload.wikimedia.org/wikipedia/commons/d/de/Nellis_AFB_Solar_panels.jpg`

[16] P.W. Sauer and M.A. Pai, *Power System Dynamics and Stability*. Upper Saddle River, New Jersey: Prentice-Hall, 1998.

[17] J. Chow, G. Rogers, "Power system toolbox version 3.0 manual", unpublished.

[18] Electricity Storage Association. (2011, May). Storage Technologies [Online]. Available: `http://www.electricitystorage.org/technology/storage_technologies/`

[19] X. Zhang et al., *Flexible AC Transmission Systems: Modeling and Control*, Berlin, Germany, Springer, March 2006.

[20] K. Rogers, "Distributed voltage support on the Smart Grid," presented at Thirty-First Annual Meeting of the Power Affiliates Program, Urbana, Illinois, 2010.

[21] J. D. Glover et al., "Power distribution," in *Power System Analysis and Design*, 5th ed. Stamford, CT: CENAGE Learning, 2012, pp. 795-799.

[22] PowerWorld Corporation. (2011, March 29). Examples and Software [Online]. Available: `http://www.powerworld.com/gloversarma.asp`

[23] *Surface vehicle recommended practice*, Society of Automotive Engineers Standard J1772, 2001.

[24] *Electric vehicle conductive charge coupler*, Society of Automotive Engineers Standard J1773, 2001.

[25] K. M. Rogers et al.,"An authenticated control framework for distributed voltage support on the smart grid," *IEEE Transactions on Smart Grid*, vol. 1, no. 1, pp. 40-47, June 2010.

[26] A. A. Aquino-Lugo et al., "A control framework for the Smart Grid for voltage support using agent-based technologies," *IEEE Transactions on Smart Grid*, vol. 2, no. 1, pp. 173-180, March 2011.

[27] M. C. Kisacikoglu et al., "Examination of a PHEV bidirectional charger system for V2G reactive power compensation," *2010 Twenty-Fifth Annual IEEE Applied Power Electronics Conference and Exposition (APEC)*, pp. 458-465, 21-25 Feb. 2010.

[28] T. Markel et al., "Value of plug-in vehicle grid support operation," *2010 IEEE Conference on Innovative Technologies for an Efficient and Reliable Electricity Supply (CITRES)*, pp. 325-332, 27-29 Sept. 2010.

[29] SEMIKRON. (2011, April 19). Semistack IGBT [Online]. Available: `http://www.semikron.com/products/data/cur/assets/SKS_65F_B2CI_08_V12_29835219.pdf`

[30] Coda Automotive. (2011, April 19). Coda Sedan Technical Specifications [Online]. Available: `http://www.codaautomotive.com/pdf/CODA_press_kit_sedan_spec_r3.pdf`